

Impacts and uncertainties of climate-induced changes in watershed inputs on estuarine hypoxia

Authors: Kyle E. Hinson¹, Marjorie A.M. Friedrichs¹, Raymond G. Najjar²; Maria Herrmann², Zihao Bian³, Gopal Bhatt^{4,5}, Pierre St-Laurent¹, Hanqin Tian⁶, Gary Shenk^{7,5}

¹Virginia Institute of Marine Science, William & Mary, Gloucester Point, VA 23062, USA

²Department of Meteorology and Atmospheric Science, The Pennsylvania State University, University Park, PA 16802, USA

³International Center for Climate and Global Change, Auburn University, Auburn, AL 36849, USA

⁴Department of Civil & Environmental Engineering, The Pennsylvania State University, State College, 16801, USA

⁵United States Environmental Protection Agency Chesapeake Bay Program Office, Annapolis, 21401, USA

⁶Schiller Institute for Integrated Science and Society, Department of Earth and Environmental Sciences, Boston College, Chestnut Hill, MA 02467, USA

⁷United States Geological Survey, Virginia/West Virginia Water Science Center, Richmond, VA 23228, USA

Correspondence to: Kyle E. Hinson (kehinson@vims.edu; kyle.e.hinson@gmail.com)

Abstract

Multiple climate-driven stressors, including warming and increased nutrient delivery, are exacerbating hypoxia in coastal marine environments. Within coastal watersheds, environmental managers are particularly interested in climate impacts on terrestrial processes, which may undermine the efficacy of management actions designed to reduce eutrophication and consequent low-oxygen conditions in receiving coastal waters. However, substantial uncertainty accompanies the application of Earth System Model (ESM) projections to a regional modeling framework when quantifying future changes to estuarine hypoxia due to climate change. In this study, two downscaling methods are applied to multiple ESMs and used to force two independent watershed models for Chesapeake Bay, a large coastal-plain estuary of the eastern United States. The projected watershed changes are then used to force a coupled 3-D hydrodynamic-biogeochemical estuarine model to project climate impacts on hypoxia, with particular emphasis on projection uncertainties. Results indicate that all three factors (ESM, downscaling method, and watershed model) are found to contribute significantly to the uncertainty associated with future hypoxia, with the choice of ESM being the largest contributor. Overall, in the absence of management actions, there is a high likelihood that climate change impacts on the watershed will expand low-oxygen conditions by 2050, relative to a 1990s baseline period; however, the projected increase in hypoxia is quite small (4%) because only climate-induced changes in watershed inputs are considered and not those on the estuary itself. Results also demonstrate that the attainment of established nutrient reduction targets will reduce annual hypoxia by about 50% compared to the 1990s. Given these estimates, it is virtually

44 certain that fully implemented management actions reducing excess nutrient loadings will
45 outweigh hypoxia increases driven by climate-induced changes in terrestrial runoff.

46

47 **Short Summary**

48

49 Climate impacts are essential for environmental managers to consider when implementing
50 nutrient reduction plans designed to reduce hypoxia. This work highlights relative sources of
51 uncertainty in modeling regional climate impacts on the Chesapeake Bay watershed and
52 consequent declines in Bay oxygen levels. The results demonstrate that planned water quality
53 improvement goals are capable of reducing hypoxia levels by half, offsetting climate-driven
54 impacts to terrestrial runoff.

1 Introduction

Over the past several decades, estuarine and coastal ecosystems have been subject to elevated levels of hypoxia relative to the open ocean (Gilbert et al., 2010), and are anticipated to be affected by multiple climate change impacts including terrestrial runoff changes (Breitburg et al., 2018) and rising temperatures (Whitney, 2022). Increases in precipitation volume and intensity are likely to increase discharge and associated nutrient and sediment export to coastal systems (Howarth et al., 2006; Lee et al., 2016; Sinha et al., 2017). Rising atmospheric temperatures will increase soil temperatures and alter evapotranspiration, soil biogeochemical cycling and plant responses (Schaefer and Alber, 2007; Wolkovich et al., 2012; Ator et al., 2022), also affecting riverine nutrient export to marine habitats. Further changes to agricultural practices driven by these same climate impacts are also likely to contribute to altered nutrient applications and subsequent soil cycling (Wagena et al., 2018). Altogether, climate impacts in the terrestrial environment may further eutrophy coastal ecosystems (Najjar et al., 2010), altering the phenology and biogeochemical rates of nutrient consumption and exacerbating hypoxia (Testa et al., 2018).

Future estimates of coastal hypoxia have increased substantially over the past decade, likely influenced by increased access to biogeochemical modeling tools and regional climate projections needed for finer scale modeling and analyses (Fennel et al., 2019). The majority of coastal hypoxia climate impact studies have focused on a select few coastal locations including the Baltic Sea (Meier et al., 2011a,b; Meier et al., 2012; Neumann et al., 2012; Ryabchenko et al., 2016; Saraiva et al., 2019a,b; Wählström et al., 2020; Meier et al., 2021; Meier et al., 2022), Chesapeake Bay (Wang et al., 2017; Irby et al., 2018; Ni et al., 2019; Testa et al., 2021; Tian et al., 2021; Cai et al., 2021), and the Gulf of Mexico (Justić et al., 1996; Justić et al., 2007; Lehrter et al., 2017; Laurent et al., 2018). Other projected changes to dissolved oxygen (O₂) levels have been documented in nearshore environments including the North Sea (Meire et al., 2013; Wakelin et al., 2020), Arabian Sea (Lachkar et al., 2019), California Current System (Dussin et al., 2019; Siedlecki et al., 2021; Pozo Buil et al., 2021), and coastal waters surrounding China (Hong et al., 2020; Yau et al., 2020; Zhang et al., 2021; Zhang et al., 2022). Hypoxia projections in relatively smaller estuaries have also been documented in the Elbe (Hein et al., 2018), Garonne (Lajaunie-Salla et al., 2018), and Long Island Sound (Whitney and Vlahos, 2021).

Broadly speaking, these climate impact studies apply either a range of idealized changes to conduct a sensitivity study or utilize long-term projections derived from Earth System Models (ESMs) (IPCC, 2013). When directly applying such projections to study regional coastal oxygen responses, dynamically or statistically downscaled estimates of atmospheric and marine variables are typically used to continuously simulate climate impacts or to calculate and apply a change factor (Carter et al., 1994; Anandhi et al., 2011) to a shorter historical time period. Quantifying the relative uncertainties from various sources including ESM, downscaling methodology, internal variability, and hydrological model is not new to the field of climate research (Hawkins and Sutton, 2009; Yip et al., 2011; Northrop and Chandler, 2014) or watershed applications (Bosshard et al., 2013; Vetter et al., 2017; Wang et al., 2020; Ohn et al., 2021). Questions of uncertainty due to climate effects in past marine ecosystem impact studies have often been addressed by selecting some combination of ESMs and/or emissions scenarios (Meier et al., 2011a; Ni et al., 2019; Saraiva et al., 2019b; Meier et al., 2019; Meier et al., 2021; Pozo Buil et al., 2021). Additionally, some studies have also sought to account for the importance of managed nutrient runoff from terrestrial (Irby et al., 2018; Saraiva et al., 2019a; Bartosova et al., 2019;

101 Pihlainen et al., 2020) and atmospheric (Yau et al., 2020; Meier et al., 2021) sources and their
102 impacts on oxygen levels. Despite some comprehensive efforts to identify sources of uncertainty
103 in coastal oxygen projections (Meier et al., 2019; 2021), few studies have evaluated uncertainties
104 introduced by the choice of specific downscaling method and/or terrestrial model. These factors
105 represent additional sources of variability when estimating future hypoxia and are inherent in
106 regional simulations of coastal dynamics.

107 The Chesapeake Bay, which is the largest estuary in the continental United States (Kemp et
108 al., 2005), has undergone intensive management efforts to improve water quality and oxygen
109 levels over the past three decades. These management efforts have focused on the reduction of
110 excess nitrogen, phosphorus, and sediment loadings to the Bay (USEPA, 2010), and continuous
111 adaptive monitoring efforts to evaluate progress in restoring water quality (Tango and Batiuk,
112 2016). Recent analyses of monitoring data have demonstrated improvements in water quality
113 throughout the Bay despite the trajectory of recovery being slowed by extreme weather events
114 (Zhang et al., 2018). Observed lags in water quality responses to nutrient reductions (Murphy et
115 al., 2022) are also evident in recent years (Zahran et al. 2022). Despite the difficulties in
116 assessing long-term improvements in water quality due to strong interannual variability, new
117 research has demonstrated that the Chesapeake Bay is more resilient to recent and ongoing
118 climate change impacts that have decreased oxygen levels as a result of decades of nutrient load
119 reductions (Frankel et al., 2022).

120 In recent years managers have recognized the importance of investigating whether the
121 originally established Total Maximum Daily Loads (USEPA, 2010) will need to be adjusted to
122 ensure the attainment of water quality standards for the Chesapeake Bay as the climate changes
123 (Chesapeake Bay Program, 2020; Hood et al., 2021). Increasing temperatures and precipitation
124 are anticipated to affect watershed snowpack, soil moisture levels, terrestrial nutrient cycling,
125 and associated discharge, streamflow generation, and flooding (Shenk et al., 2021b), potentially
126 altering the efficacy of nutrient reduction strategies. Increases in nutrient and carbon inputs to the
127 Bay resulting from climate change and anthropogenic stressors have already been documented
128 over the course of the past century (Pan et al., 2021; Yao et al., 2021), and are anticipated to
129 increase in the 21st century as well (Wang et al., 2017; Irby et al., 2018; Ni et al., 2019). For
130 example, Irby et al. (2018) directly tested the role of future nutrient reductions via a sensitivity
131 analysis of mid-century climate effects, and found substantial alleviation of hypoxic conditions
132 when management targets were met, despite significantly increasing water temperatures.
133 However, that study applied spatially constant changes in watershed inputs derived from a
134 specific watershed model, one downscaling technique and a median estimate of ESM
135 projections. A more robust effort to produce a range of scenarios incorporating multiple
136 watershed models, downscaling techniques and ESMs is needed to assess uncertainty estimates
137 of projected hypoxia, which can be used to guide decision-making that explicitly considers what
138 levels of environmental risk are acceptable for Chesapeake Bay stakeholders.

139 The present study applies multiple downscaled ESMs to two independently developed
140 watershed models with significantly different representation of watershed processes and spatial
141 scale; both are used to force a coupled hydrodynamic-biogeochemical estuarine model in order
142 to better constrain the relative uncertainties of future terrestrial runoff estimates on estuarine
143 hypoxia (Shenk et al., 2021a). The resulting ensemble of numerical experiments includes
144 realistic climate forcings and an extensive set of regional linked watershed-estuarine
145 deterministic model simulations. The framework established in this research assesses the relative
146 uncertainties introduced by choice of ESM, downscaling methodology, and regionally focused

147 watershed model in quantifying changes to O₂ levels in the estuary. Additionally, this
148 investigation constrains the bounds of changes to Chesapeake Bay hypoxia (defined herein as O₂
149 < 2 mg L⁻¹) with and without the effects of management actions, using an ensemble of realistic
150 watershed forcings. The study provides a roadmap for environmental managers to design climate
151 impact assessments that are better able to quantify the range of possible future levels of hypoxia,
152 which can be influenced by nutrient management actions.

153

154 **2 Methods**

155

156 **2.1 Monitoring data**

157 Monthly estimates of freshwater discharge, inorganic nitrogen, and organic nitrogen at the
158 non-tidal monitoring stations nearest the head of tide of the three largest tributaries to the
159 Chesapeake Bay (Susquehanna, Potomac, and James; Fig. 1a; Table S1) were used to evaluate
160 the performance of watershed models. Discharge and nitrogen load estimates are derived from
161 observations that are collected at United States Geological Survey (USGS) stream gages and
162 comprise part of the USGS River Input Monitoring program in the Chesapeake Bay watershed.
163 Estimates for the nitrogen species were calculated using a weighted statistical regression process
164 that accounts for the variability introduced by time, discharge, and season (Hirsch et al., 2010).

165 Main stem bay observations collected over the period 1991-2000, accessible via a data
166 repository maintained by the Chesapeake Bay Program (CBP; Olson 2012; CBP DataHub 2020),
167 were used to assess estuarine model skill (see Sect. 2.3.1). Since 1984, numerous water quality
168 data have been collected along the Bay's main stem and throughout its tributaries at semi-
169 monthly to monthly intervals as part of the Water Quality Monitoring Program. These data were
170 collected at the surface, above and below the pycnocline, and at the bottom for chemical
171 variables including nitrate and organic nitrogen, and throughout the entire water column at 1-2 m
172 intervals for O₂. Twenty CBP stations were selected for model comparison at the surface and
173 bottom (Fig. 1b, Table S2), including those most frequently sampled and those located along the
174 entirety of the Bay's main channel where hypoxia commonly occurs (Officer et al., 1984; Hagy
175 et al., 2004). Estimates of annual hypoxic volume (AHV), defined as the volume of hypoxic
176 water integrated over the year (with units of volume*time), were taken from the Bever et al.
177 (2013; 2018; 2021) interpolation of O₂ measurements at 56 CBP stations.

178

179 **2.2 Estuarine and watershed modeling tools and evaluation**

180 Model simulations are conducted with ChesROMS-ECB, a fully coupled, three-dimensional,
181 hydrodynamic and Estuarine Carbon Biogeochemistry (ECB) implementation of the Regional
182 Ocean Modeling System (ROMS ; Shchepetkin and McWilliams 2005) developed for the
183 Chesapeake Bay (Xu et al., 2011) with 20 terrain-following vertical levels and an average
184 horizontal resolution of approximately 1.8 kilometers in the estuary's mainstem (Feng et al.,
185 2015; St-Laurent et al., 2020; Frankel et al., 2022). Two parameter changes were recently made
186 to improve the representation of modeled oxygen: (1) a decrease of the maximum growth rate of
187 phytoplankton, which, following Irby et al. (2018), preserves the temperature-dependent linear
188 Q₁₀ described in Lomas et al. (2002), and (2) a decrease in the critical bottom shear stress from
189 0.010 Pa to 0.007 Pa, which increases the resuspension of organic matter and is well within the
190 range of observed shear stresses evaluated by Peterson (1999).

191 Estimates of watershed discharge, nitrogen loading, and sediment loading to drive the
192 estuarine model were obtained via two independently developed models of the Chesapeake Bay

193 watershed: the Dynamic Land Ecosystem Model (DLEM; Yang et al., 2015; Yao et al., 2021)
194 and the USEPA Chesapeake Bay Program’s regulatory Phase 6 Watershed Model (Phase 6;
195 Chesapeake Bay Program, 2020). Both models were applied to generate comparable reference
196 runs over the average hydrology period of 1991-2000, chosen because it reflects the decade used
197 by the Chesapeake Bay Program to calculate Total Maximum Daily Loads (USEPA, 2010) and
198 assess water quality improvements. Outputs from both watershed models were aggregated into
199 10 major river input locations (Fig. 1). Watershed outputs were mapped to estuarine variables as
200 in Frankel et al. (2022), except that a more realistic partitioning of terrestrial organic nitrogen
201 loading into labile and refractory pools was implemented such that the percent refractory organic
202 nitrogen loading increases with discharge at high flow volumes (Appendix A).

203 Atmospheric conditions, including temperature and winds, were obtained from the ERA5
204 reanalysis dataset (C3S, 2017) as in Hinson et al. (2021). Coastal boundary conditions were
205 interpolated to match the nearest physical and nutrient observations, as in previous work (Da et
206 al., 2021). In order to isolate the impacts of climate-driven changes in watershed inputs,
207 atmospheric and coastal boundary conditions were kept the same in all model simulations under
208 realistic 1991-2000 conditions, for both reference runs (1991-2000) and all future scenarios
209 (2046-2055).

210 Watershed and estuarine model skill was evaluated by comparing results from the two
211 reference scenarios to available data (see Sect. 2.1). Nash–Sutcliffe efficiencies (Nash and
212 Sutcliffe, 1970) were used to evaluate watershed model performance of freshwater discharge and
213 nutrient loadings. Estuarine model skill was evaluated by comparing model outputs matching the
214 spatio–temporal variability of observations at 20 main stem stations over the 10-year reference
215 period. Average bias (model output minus observed value) and root-mean squared difference
216 (RMSD) of annual O₂, nitrate (NO₃), and dissolved organic nitrogen (DON) concentrations were
217 calculated at the surface and bottom. AHV estimates were calculated by summing the daily
218 volume of model cells containing low-oxygen waters (O₂ < 2 mg L⁻¹), and are expressed in units
219 of km³ d following Bever et al. (2013; 2018; 2021). Daily net primary production estimates were
220 integrated over the entire water column and averaged across the Bay and month before being
221 compared to average Bay-wide estimates from Harding et al. (2002).

222

223 **2.3 Projected changes in atmospheric temperature and precipitation**

224 Mid-21st century projected changes in atmospheric temperature and precipitation under a
225 high emissions scenario (RCP 8.5) were obtained for multiple CMIP5 ESMs that were regionally
226 downscaled via two statistical methodologies: Multivariate Adapted Constructed Analogs
227 (MACA; Abatzoglou and Brown, 2012; downloaded from MACAv2-METDATA) and Bias-
228 Correction and Spatial Disaggregation (BCSD; Wood et al., 2004; downloaded from
229 Reclamation, 2013). (Note that downscaled CMIP5 ESM output was used because downscaled
230 CMIP6 ESM output was not yet available when the research began.) Downscaled MACA and
231 BCSD projections have an average spatial resolution of approximately 0.042° and 0.125°,
232 respectively. A delta approach (Prudhomme et al., 2002; Anandhi et al., 2011) was used to
233 estimate the absolute change in atmospheric temperature and fractional change in precipitation
234 over the Chesapeake Bay watershed. In this delta approach (also commonly referred to as a
235 perturbation method or change-factor method), the difference in a given climate variable (i.e., air
236 temperature or precipitation) is calculated by first subtracting monthly downscaled ESM
237 estimates averaged over a hindcast period (in this case 1981-2010) from average monthly future
238 projections (in this case 2036-2065). The resulting mean annual cycle (with monthly resolution)

239 in the delta (i.e., the absolute change in temperature or fractional change in precipitation) is then
240 applied to reference atmospheric forcing inputs (in this case for 1991-2000) to generate future
241 watershed scenarios (in this case for 2046-2055, hereafter referred to as mid-century) and limit
242 uncertainty introduced by interannual variability. An additional step to modify precipitation
243 intensity is also included in all climate scenarios, following the methodology outlined in Shenk
244 et al. (2021b). Thirty-year averaging periods were used to limit potential biases introduced by
245 multidecadal oscillations.

246 To reduce the computational load of applying the dozens of available ESMs to our combined
247 watershed-estuarine modeling framework for a full factorial experiment, the Katsavounidis-Kuo-
248 Zhang (KKZ; Katsavounidis et al., 1994) algorithm was applied to select a subset of five ESMs
249 from both downscaled datasets. KKZ is an objective procedure for selecting a subset of members
250 that best span the spread of the full ensemble in a multivariate space. Because changes to
251 hypoxia must be computed after a subset of ESMs are selected, the downscaled results were
252 classified in terms of changes to the two variables most likely to influence hypoxia: air
253 temperature from May–October (i.e., the historic hypoxic season in Chesapeake Bay) and
254 precipitation from November–June (corresponding to the highest set of correlation coefficients
255 when regressed against historical AHV estimates; Supplementary Material; Fig. S1). The KKZ
256 algorithm first selected an ESM nearest to the center of the cluster of models in the two-
257 parameter space, which is referred to hereafter as the Center ESM, before iteratively selecting
258 additional ESMs that were furthest from the center of the distribution and other previously
259 selected ESMs (Fig. 2, Table S3). The next four selected ESMs are referred to as Hot/Wet,
260 Cool/Wet, Hot/Dry, and Cool/Dry ESMs to denote whether they are cooler, hotter, wetter, or
261 drier, relative to the Center ESM. The specific ESMs selected based on MACA and BCSD differ
262 slightly; however, three of the five models are the same (Cool/Dry, Hot/Dry, and Cool/Wet). The
263 selection process incrementally adds members to those previously selected, so that the entire
264 ensemble is ordered and a subset of any size can be selected. This method has proven effective at
265 covering the largest range of outcomes using the fewest ESMs in watersheds across the United
266 States in previous research (Ross and Najjar, 2019). This ESM selection process allows for a
267 more robust comparison of the distribution of ESMs from multiple downscaled datasets as
268 opposed to individual ESM comparisons that may privilege one downscaling method over
269 others. However, because inexact matches among ESMs can impact the quantification of relative
270 uncertainty (Sect. 2.5), additional scenarios were simulated as needed for the Center and
271 Hot/Wet ESMs, which were different for the two downscaling techniques (Fig. 2, Table S3).
272 Future change in temperature and precipitation between the two downscaling methods are shown
273 for the Center ESM (Fig. 3); changes for the other four ESMs are found in the Supplementary
274 Material (Fig. S2).

275 276 **2.4 Experiments**

277 Three numerical experiments (sets of simulations) were conducted to evaluate the impacts of
278 climate scenario factors, management conditions, and the use of a subset of ESMs on future
279 AHV projections and uncertainty (Table 1). To isolate climate impacts on AHV from the
280 watershed alone, direct atmospheric and oceanic forcings to the Bay were held the same as in the
281 reference simulations (see Sect. 2.3) for all experiments. The first experiment (Multi-Factor)
282 evaluates the relative change in AHV (hereafter defined as Δ AHV) between the 1991-2000 and
283 2046-2055 time periods due to the following factors: ESM, downscaling method, and watershed
284 model (Table 1, Fig. 4). Atmospheric deltas from ten downscaled ESMs (five from MACA and

285 five from BCSD) were applied directly to the two watershed models for a total of 20 simulations.
286 A separate Phase 6 climate-reference run is used to evaluate the impacts of climate alone by
287 holding land use and nutrient applications constant. This differs slightly from the Phase 6
288 reference run that simulates realistic and interannually varying nutrient inputs and terrestrial
289 conditions and is compared against observations (Sect. 2.2). Two additional simulations were
290 conducted with Phase 6 to account for the fact that the ESMs selected by the KKZ method were
291 not identical for MACA and BCSD (Table 1, Fig. 2).

292 The second experiment (Management) applied the same deltas used for Phase 6 MACA
293 scenarios in the Multi-Factor experiment (thereby varying runoff and nutrient loading), but also
294 included the effect of changing environmental management conditions (affecting nutrient inputs
295 to and export from the terrestrial environment), for a total of five additional simulations. These
296 Management simulations assume that reduction targets for nutrient and sediment runoff are met
297 in accordance with established management goals (USEPA, 2010). One additional scenario was
298 conducted in which management goals were imposed, and climate change was not.

299 The third experiment (All ESMs) applied all 20 MACA downscaled ESM deltas to the
300 DLEM scenarios without any changes to management conditions, thereby only modifying
301 changes in runoff and nutrient export without intentional nutrient reductions, for a total of 20
302 additional simulations. Comparing the results of the first (Multi-Factor) and third (All ESMs)
303 experiments highlights the strengths and limitations of using a subset of ESMs.

304

305 **2.5 Climate scenario analyses**

306 To analyze climate impacts on Chesapeake Bay hypoxia, changes in O₂ and AHV were
307 compared between the reference runs and the future simulations. Relative O₂ impacts introduced
308 by the three climate scenario factors (ESM, downscaling method, and watershed model) were
309 determined by applying an analysis of variance (ANOVA) approach to average Δ AHV estimates
310 for each climate scenario. This method has been previously applied to the quantification of
311 uncertainty sources in climate and hydrological applications (Hawkins and Sutton, 2009; Yip et
312 al., 2011; Bosshard et al., 2013; Ohn et al., 2021). To use this method in this study, an average
313 annual metric is first calculated for an outcome of interest (i.e., change in discharge, nitrogen
314 loading, or hypoxic volume) within the Multi-Factor experiment. Then, the relative uncertainty is
315 determined by calculating the sum of squares due to individual effects for each experimental
316 factor (ESM, downscaling method, or watershed model). Following Ohn et al. (2021), the
317 cumulative uncertainty is quantified for successive uncertainties introduced by each factor as
318 well as their interactions, removing the unexplained interaction term described in Bosshard et al.
319 (2013). The two additional ESM scenarios described previously (Table 1, Table S3) were used
320 due to the inexact matches between MACA and BCSD ESMs selected by KKZ. Despite five
321 ESMs being used in combination with only two downscaling methods and two watershed models
322 in this analysis, the approach outlined (Bosshard et al., 2013; Ohn et al., 2021) accounts for this
323 factor imbalance (five vs. two) by repeatedly subsampling combinations of two ESM scenarios
324 from the five available. An example of this methodological approach is described in Appendix B.

325 Relative frequency histograms and cumulative distributions were used to quantify the overall
326 likelihoods of increasing/decreasing Δ AHV across the entire range of future scenarios. Average
327 changes in the spatial distribution of O₂ over the typical hypoxia season (May–September) were
328 compared among all climate scenarios with no changes to management conditions. Results were
329 considered significant if at least 80% of model scenarios tested agree on the direction of O₂
330 change in the estuary, as in Tebaldi et al. (2011).

331
332
333
334
335
336
337
338
339
340
341
342
343
344
345
346
347
348
349
350
351
352
353
354
355
356
357
358
359
360
361
362
363
364
365
366
367
368
369
370
371
372
373
374
375
376

3 Results

3.1 Model Skill

3.1.1 Watershed Models

Modeled discharge, nitrate loading, and organic nitrogen loading from the three largest Bay tributaries are comparable to observed monthly estimates derived from weighted statistical regressions (see Sect. 2.1). At the most downstream USGS stations on the Susquehanna, Potomac, and James Rivers, both Phase 6 and DLEM discharge estimates have higher skill (Nash–Sutcliffe Efficiencies closer to 1.0) relative to nitrate and organic nitrogen loading estimates (Table 2, Fig. S3). Although the overall skill of Phase 6 and DLEM is similar, Phase 6 generally exhibits higher model skill than DLEM in estimating monthly nitrate loading, while DLEM demonstrates greater skill in simulating organic nitrogen loading.

3.1.2 Estuarine Model

The two reference simulations, forced with loadings from DLEM and Phase 6, demonstrate substantial skill in representing key main stem estuarine biogeochemical variables, including O₂, NO₃, DON, primary production, and AHV (Table 3) throughout the Bay’s mainstem. Overall, all modeled variables at the surface and bottom forced by both DLEM and Phase 6 lie within 1 standard deviation of observations. Modeled O₂ is slightly greater than spatio–temporally paired observations at the bottom, and slightly lower than observations at the surface throughout the entire year (Table 3) and in the summer period of hypoxia (Fig. 5a-b), leading to a bias that is relatively small compared to the standard deviations of observed O₂ concentrations across the entire year (Table 3). Additionally, modeled O₂ performs similarly to or better than the results included in the multi-model comparison presented in Irby et al. (2016). Modeled average annual NO₃ and DON are also within the range of observations at both the surface and bottom (Table 3). Whole Bay net primary production agrees well with observed estimates (Harding et al., 2002) reported over a similar time period (Table 3). Finally, modeled AHV compares favorably to data-derived interpolated estimates (Table 3; Fig. 5c), with increased hypoxia in wet years compared to dry years. Average AHV estimates using Phase 6 and DLEM inputs are, respectively, 16% and 26% greater than interpolated observations (Table 3; Fig. 5c) and approximately half the model estimates lie within the estimated uncertainties (RMS % error) of the interpolation methodology ($\pm 13\%$; Bever et al., 2018). Model estimates of AHV are generally slightly greater when ChesROMS-ECB is forced by DLEM watershed outputs as opposed to those from Phase 6 (Table 3; Fig. 5c).

3.2 Future (mid-21st century) projections of watershed discharge and nutrient loading

Increasing temperatures and changing precipitation throughout the Bay watershed produce different discharge responses for the two watershed models. On average, Phase 6 climate scenarios increase watershed runoff relative to the reference run by 4-6% while DLEM climate scenarios decrease average flow by 1-4% (Table 4). The annual flow changes range from -12 to +15% among ESM scenarios, with wetter ESMs tending to increase annual watershed discharge

377 while drier ESM scenarios generally decrease average watershed runoff, with a lesser impact due
378 to atmospheric warming (Table 4; Fig. 6a). For both watershed models and downscaling
379 methods, the Cool/Wet ESM produces the greatest increase in annual discharge. Overall, the
380 greatest variability in changes to discharge estimates is due to ESM, as MACA and BCSD
381 scenarios increase or decrease annual discharge by comparable amounts (Table 4; Fig 6a).

382 Chesapeake Bay Phase 6 watershed model climate scenarios increase average annual total
383 nitrogen (TN) by +30% and +45% for MACA and BCSD respectively, but do not substantially
384 change DLEM TN loads (+1% and -2% for MACA and BCSD, respectively; Fig. 7). Greater
385 Phase 6 TN loadings are primarily due to extreme values in the Cool/Wet climate scenarios and
386 are driven by increases in refractory DON (Fig. 7a). While DLEM scenarios show increases in
387 the percentage of inorganic nitrogen and labile organic forms of total nitrogen loads, the
388 contribution of particulate organic nitrogen (PON) decreases, resulting in little to no increases in
389 overall TN loading (Fig. 7a). Phase 6 produces wetter climate scenarios increasing TN loading
390 more than drier scenarios (Table 4; Fig 6b), with this effect being most pronounced for the
391 Cool/Wet ESM. Phase 6 also produces the greatest percent changes in the southern rivers (James,
392 York, Rappahannock), while DLEM produces similar percent changes in all rivers (Fig. 7b).
393 Some Phase 6 climate scenarios substantially increase the average loading change in smaller
394 watersheds like the Rappahannock and York, which increase TN between 77-172% and 32-
395 430%, respectively, and are comparable to the absolute change in Susquehanna TN loading (Fig.
396 7b). In contrast with the Multi-Factor experiment results, climate scenarios that include
397 management actions substantially reduce TN loading (-28%; Fig. 7, Table 4). Like other Phase 6
398 climate scenarios that don't account for management actions, the proportion of refractory organic
399 nitrogen increases for the climate scenarios with management (+49%), but in these cases the
400 average labile inorganic and organic nitrogen loadings also substantially decrease (-40%).

401

402 **3.3 Effects of future watershed change on estuarine O₂**

403

404 Climate change impacts on watershed discharge and nitrogen loading substantially affect
405 estuarine hypoxia, even when, as in this study, direct climate effects on the Bay are not
406 considered. On average, the Multi-Factor climate scenarios decrease average summer bottom O₂
407 in the Bay's mainstem while also slightly increasing O₂ at the surface in some mid-Bay areas
408 (Fig. 8). In the northern part of the mainstem near the Susquehanna River outfall, model results
409 show consistent decreases in both bottom and surface summer O₂ (Fig. 8e,f). Further down the
410 main stem in the mid-Bay, surface O₂ increases in wet years, and experiences almost no change
411 in dry years (Fig. 8b,c). In the same region, bottom O₂ declines less during wet years and
412 worsen during dry years (Fig. 8e,f). Increasing O₂ levels are found in the shallow portions of the
413 major tidal tributaries (i.e., Potomac and James), but are more pronounced in wet years than dry
414 years (Fig. 8b-c,e-f). Altogether, average summer surface O₂ increases by $0.02 \pm 0.03 \text{ mg L}^{-1}$
415 (average change and standard deviation) while bottom O₂ decreases by $0.03 \pm 0.06 \text{ mg L}^{-1}$.

416 There are some clear distinctions in the overall changes to future AHV when evaluating all
417 Multi-Factor experiments. Climate effects on the watershed in DLEM increase AHV more so
418 than in Phase 6 (5.6% vs 3.1%, respectively), but the overall standard deviation of DLEM Δ AHV
419 results are greater than those for Phase 6 (Table 5). Similarly, using MACA vs. BCSD results in
420 greater changes in Δ AHV (4.8% vs. 3.9%), albeit this difference due to the choice of
421 downscaling method is less than that due to the choice of watershed model. Depending on the
422 choice of ESM, Δ AHV ranges between +0.9% (for the Cool/Dry ESM) to +8.3 % (for the

423 Cool/Wet ESM) with the Center ESM producing intermediate results (+4.4 %). When comparing
424 the impact of a particular ESM, wetter models tend to produce greater Δ AHV than drier
425 scenarios (Fig. 6c), although interannual variability is still large. When climate scenarios are
426 downscaled using different methodologies (either MACA or BCSD), average Δ AHVs have some
427 notable differences, e.g., applying the Cool/Dry model to Phase 6 produces opposite average
428 changes to hypoxia depending on downscaling method (Fig. 6c). Considering all possible
429 combinations of scenarios, ESM average annual projected AHV spans a range of 921-939 km³ d
430 for Phase 6 and 1019-1049 km³ d for DLEM, and four out of five of the climate scenarios in the
431 Multi-Factor experiment projecting increases in average AHV (Table 4).

432 When the full distribution of Multi-Factor scenarios is evaluated, the average and standard
433 deviation of these annual Δ AHV results are estimated to be 37 ± 64 km³ d ($4.4 \pm 7.4\%$; Fig 9).
434 Wetter ESMs (blues in Fig. 9a) are more likely to increase hypoxia compared to drier ESMs,
435 despite differences in downscaling method or watershed model. The likelihoods of the Cool/Dry
436 or Hot/Dry ESM increasing hypoxia are only 58% or 50%, respectively, but these chances are
437 greater than 80% for the Center, Hot/Wet, and Cool/Wet ESMs (Fig. 9a). Altogether, the Multi-
438 Factor experiment results in 72% of the runs increasing AHV when considering climate change
439 impacts on terrestrial runoff (Fig. 9b). (Note, however, that this cannot technically be considered
440 to be a statistical probability as the KKZ selection process used to generate our sample of climate
441 scenarios is neither random nor independent.)

442 The All-ESMs experiment produces similar results to those obtained when only a subset of
443 five ESMs are used. Specifically, Δ AHV increases by $6.3 \pm 3.5\%$ using only five KKZ-selected
444 ESMs and by $9.6 \pm 1.7\%$ when using all 20 ESMs (Fig. 10a,b; Model IDs further defined in
445 Table S3). The use of five KKZ-selected ESMs covers approximately 69% of the total range of
446 all 20 ESMs (Fig. 10c). Despite more than 15,000 options to choose from when selecting five out
447 of 20 ESMs, the subset selected in this work demonstrates an improved ability to outperform a
448 random selection of five ESMs (Fig. 10c) and generates a useful range of hypoxia projections.

449 The results of the Management experiment demonstrate the substantial impact of future
450 nutrient reductions on hypoxia, decreasing average AHV by $50 \pm 7\%$ relative to the 1990s
451 (Δ AHV = -438 ± 47 km³ d; Table 4; Fig. 11). Because there is a linear relationship between
452 Δ AHV computed with Phase 6 MACA scenarios including management actions (Δ AHV_{mgmt}) and
453 those without (Δ AHV = $0.56 * \Delta$ AHV<sub>mgmt} - 262; $R^2=0.59$, Fig. S5), Δ AHV_{mgmt} can be estimated
454 for any scenario by applying this linear model to the non-management scenario distribution. In
455 effect, this linear relationship demonstrates a similar magnitude of relative nutrient export to and
456 consequent hypoxia within the estuary. The result is a decrease of approximately 417 ± 67 km³ d
457 among all scenarios, within the range of the management scenario subset obtained here by
458 applying only MACA downscaled ESMs to Phase 6. As expected, hypoxia increases in the
459 Management experiment when climate impacts are also included relative to the reference
460 management scenario, specifically by 17.1 ± 34.8 km³ d or $3.8 \pm 7.8\%$ (Table 4; Fig 6c).</sub>

461

462 **3.4 Contributions to Climate Scenario Uncertainty**

463

464 Applying an ANOVA approach (Ohn et al., 2021) to watershed discharge, nutrient loadings,
465 and Δ AHV within the Multi-Factor experiment reveals that the relative uncertainties introduced
466 by the choice of ESM, downscaling method, and watershed model vary substantially (Fig. 12).
467 The choice of ESM is the dominant factor affecting changes to watershed discharge and nutrient
468 loadings (Fig. 12a-c), and comprises 59-74% of the total uncertainty. The choice of watershed

469 model is the next largest source of uncertainty, making up 17-34% of the total variance in
470 watershed changes, while the downscaling method only contributes 3-14%. Uncertainty in
471 projected organic nitrogen loadings is particularly affected by the choice of watershed model,
472 overwhelming the variability introduced by downscaling method, and strongly affecting
473 estimates of total nitrogen change. Unlike changes to watershed flow and loadings, the
474 uncertainty of projected changes to hypoxia is much more evenly distributed among the three
475 scenario factors: 40%, 25%, and 35%, for ESM, downscaling method, and watershed model
476 respectively (Fig. 12d).

477

478 **4 Discussion**

479

480 **4.1 Uncertainty in Climate Scenario Projections**

481

482 Projected changes in watershed discharge and nutrient delivery to the Chesapeake Bay
483 produce modest increases in estuarine hypoxia, with medium confidence (Mastrandrea et al.,
484 2010). Hypoxic volume has a high degree of interannual variability, and future hypoxia estimates
485 are highly sensitive to the choice of ESM, downscaling method, and watershed model (Fig. 6c).
486 While certain factors (particularly ESM and greenhouse gas emissions scenarios; Meier et al.,
487 2021) have previously been extensively evaluated in coastal systems with regards to future
488 hypoxia, the results presented here also demonstrate the importance of terrestrial forcings on
489 estuarine oxygen levels.

490 In this study, future changes in watershed discharge, nitrogen loadings, and estuarine hypoxia
491 are found to be highly dependent on the selection of a specific ESM (Fig. 12), comprising a
492 majority of the total uncertainty in watershed runoff and the greatest fraction of total uncertainty
493 for O₂ levels. When only the effect of ESM choice is considered (and downscaling and
494 hydrological model options are not; Fig. 10), the average projected change in AHV using only
495 three ESMs (often chosen to represent cool, median, and hot scenarios) has a greater standard
496 error than the selection of five in this study. Directly comparing results from the experiment that
497 compared five ESMs, two downscaling methods, and two watershed models (Multi-Factor)
498 versus that which only considered the impact of multiple ESMs (All ESMs) shows a substantial
499 overlap in the range of projected Δ AHV. In addition, multiple ESMs downscaled with a single
500 methodology and applied to one hydrological model produced meaningfully different estimates
501 of Δ AHV than a more balanced approach (Fig. 11).

502 Inter-model variability among ESMs appears to contribute most substantially to differences
503 in Bay watershed inputs, but the choice of downscaling methodology can also affect these
504 projections. The BCSD (Wood et al., 2004) and MACA (Abatzoglou and Brown, 2012)
505 downscaling methodologies used here employ different approaches to reduce historical ESM
506 biases, impacting the variability of spatio-temporal watershed hydrologic and water quality
507 responses. The ability to statistically downscale ESMs accurately depends on the spatially
508 coarser ESM's ability to simulate synoptic-scale (~1000 km) patterns and may still
509 underestimate the distributional tails of changes to temperature and precipitation. This increases
510 the importance of properly selecting a subset of ESMs (Abatzoglou and Brown, 2012).

511 Watershed model variability is caused by differences in the representation of processes that
512 affect discharge, those controlling the fate and transport of nutrients from land and in rivers, and
513 lag times of groundwater transport. The two watershed models used here project substantially
514 different results in watershed discharge and nitrogen delivery, even when the same changes to

515 meteorological forcings are applied (Fig. 6). DLEM projects no change or decreases in discharge
516 for nearly all scenarios, as opposed to greater average increases in discharge for Phase 6
517 scenarios (Fig. 6a), likely driven by differences in the representation of evapotranspiration.
518 Explicit soil biogeochemical processes within DLEM increase nitrification rates in warmer
519 climate scenarios, producing higher nitrate loadings than Phase 6 despite comparable discharge
520 changes (Fig. 6b). The greater total nitrogen loadings produced by Phase 6 are largely a
521 consequence of its parameterizations for erosion and refractory nitrogen bound to sediment.
522 Increases in bioavailable nitrate loadings, unlike refractory organic nitrogen that comprises the
523 majority of DON loadings, produce greater levels of primary production and remineralization
524 within the estuary. This largely explains the discrepancy between watershed model hypoxia
525 estimates (Table 5).

526 Our findings demonstrate the importance of considering differences among these three
527 factors (ESM, downscaling, and watershed model) that may contribute to a wider range of target
528 water quality variables and living resource responses in coastal marine ecosystems like the
529 Chesapeake Bay that are highly influenced by watershed processes. Hydrological model
530 assumptions can have potentially significant impacts on estuarine hypoxia. For example, the
531 relatively high organic nitrogen loadings in Phase 6 compared to DLEM's comparatively modest
532 exports under the same future scenarios result in different levels of annual hypoxia. While
533 dramatic increases in organic nitrogen loadings within Bay tributaries are mostly limited to
534 Cool/Wet Phase 6 scenarios, there is precedent for catastrophic erosion within the Bay watershed
535 driven by extreme precipitation events (Springer et al., 2001). The relative uncertainty
536 introduced by individual factors is also not necessarily equivalent for discharge, nitrogen
537 loadings, and AHV (Fig. 12). The complex connections between terrestrial runoff and
538 biogeochemical changes in the marine environment may expand further when higher order
539 trophic-level species are considered, and even more so when direct atmospheric impacts on the
540 Bay are also included. It is unlikely that general conclusions regarding the relative impacts of
541 different factors can be drawn for a marine ecosystem when only uncertainties in watershed
542 discharge and nutrient loadings are considered. Had our results only accounted for the impacts of
543 these factors on watershed changes and not estuarine oxygen levels, the role of downscaling
544 could be incorrectly assumed to contribute negligible variability to hypoxic volume (Fig. 12). It
545 is the complex interactions of nitrogen species transformations within this estuarine model that
546 are responsible for this somewhat unexpected large contribution of downscaling method
547 uncertainty that is less prominent in watershed changes.

548 Despite the relatively small magnitude of Chesapeake Bay watershed climate impacts on
549 estuarine hypoxia compared to previous evaluations of other climate impacts, like atmospheric
550 warming over the Bay (Irby et al., 2018; Ni et al., 2019; Tian et al., 2021), the relative
551 contributions of ESM and downscaling effects to the total uncertainty are large and are also
552 likely to expand the range of outcomes for other climate sensitivity studies in this region. This
553 suggests that, when attempting to determine a likely range of ecosystem outcomes, selecting
554 additional downscaling techniques and hydrological model responses should be considered in
555 addition to the more common practice of only selecting multiple ESMs.

556

557 **4.2 Watershed Climate Scenario Impacts on Riverine Export and Hypoxia**

558

559 The climate scenario projections evaluated in this study are in near complete agreement that
560 the Chesapeake Bay watershed will be warmer and experience greater levels of precipitation by

561 mid-century, yet these results are not as straightforward to interpret as they relate to changes in
562 discharge, nutrient loads, and estuarine hypoxia. Climate impacts on extreme river flows are
563 currently evident at global scales (Gudmundsson et al., 2021), and projected increases in
564 precipitation that could shape such events are aligned with estimates for this region derived from
565 observational (Yang et al., 2021) and modeling (Huang et al., 2021) studies, as well as for other
566 regions at similar latitudes (Bevacqua et al., 2021; Madakumbura et al., 2021). However,
567 differences exist in the spatial distribution and timing of these precipitation increases, as well as
568 in the temperature-affected rates of evapotranspiration. As a result, these estimates produce
569 varied projections for future freshwater discharge. These complex interactions make it difficult
570 to directly predict future discharge from projected precipitation changes, and even more difficult
571 to relate these to changes in nutrient loading. For example, in this study half of the climate
572 scenarios produce increasing discharge on an annual basis, yet more than 75% of these scenarios
573 increase total nitrogen loading. Differences in the representation of soil and riverine nitrogen
574 processes between watershed models also results in inconsistent simulated responses of nitrogen
575 export to similar precipitation rates. Disparate export of nitrogen species (i.e., nitrate and organic
576 nitrogen) between watershed models also directly affects future nutrient load projections. These
577 hydrological model differences are evidenced by DLEM's higher NO_3 outputs that offset lower
578 organic nitrogen loadings (Fig. 7a), and are discussed further in depth in Sect. 4.2.

579 Our analysis quantifies changes in hypoxia due to mid-century climate change impacts on the
580 watershed, and provides an estimate of the relative uncertainty in these estimates. Our
581 experimental findings suggest that, in the absence of management actions, mid-century climate
582 impacts on the Chesapeake Bay watershed will increase hypoxia, specifically annual hypoxic
583 volume (AHV), by an average of $4 \pm 7\%$. This estimate is in good agreement with prior studies
584 that examined the impacts of watershed actions alone. Irby et al. (2018) applied a sensitivity
585 approach and projected increases in AHV of 5%, while Wang et al. (2017) showed increases in
586 annual anoxic volume of 9.7%, nearly equivalent to an increase of $10 \pm 16.5\%$ found here (Table
587 6). Results from this study also project that changes to Bay O_2 levels will vary spatially. Average
588 bottom main stem O_2 levels from May–September are expected to decrease most in the southern
589 half of the Bay (south of 38.5°N), particularly in climatologically dry years (Fig. 8).

590 Importantly, the projected changes presented here only account for the effects of climate
591 change on watershed response in isolation, and do not include the additional direct impacts of the
592 atmosphere and ocean. These additional changes have been estimated in other previous studies of
593 21st century impacts relative to observed conditions (Table 6). While numerous differing metrics
594 have been reported for many of these studies, including shifting dissolved oxygen concentrations
595 and water quality regulatory criteria, this work can be compared against previous results by
596 examining changes to annual hypoxic and anoxic volumes. The majority of these studies (Table
597 6) apply idealized changes to climate forcings and generally project increases in hypoxic
598 conditions. Increases in mid-21st century annual hypoxic volume due to watershed forcings
599 ($+5\%$ and $+4.4 \pm 7.4\%$) are smaller than average impacts of increasing temperatures alone
600 ($+13\%$), while the results of changing sea level are more mixed (Table 6). However, the
601 variability in hypoxia due to watershed changes is likely greatest among these factors and may
602 substantially modify the negative effects of warming on dissolved oxygen concentrations. Our
603 results and their uncertainties generally encompass the range of future hypoxia estimates found
604 in previous research that have studied multiple climate impacts in isolation and in various
605 combinations. Future work that accounts for the sources of uncertainty explored here by applying
606 realistic climate change projections while also standardizing a metric for model results, like

607 annual hypoxic volume, will help to narrow and better quantify definitive trends due to multiple
608 factors that influence Bay dissolved oxygen.

609 Our findings are focused on Chesapeake Bay hypoxia, but some lessons can also be drawn
610 from other coastal ecosystems where changes in watershed discharge and nutrient loadings are
611 also projected. In the Baltic Sea, Meier et al. (2011b) reported that hypoxia was very likely to
612 increase regardless of ESM or climate scenario, assuming targeted reductions in accordance with
613 the Baltic Sea Action Plan (decrease of nitrogen loads by $23 \pm 5\%$) were not met. Extensive
614 studies of projected oxygen change in the Baltic Sea have repeatedly demonstrated that climate
615 impacts are likely to increase hypoxic area (BACC II, 2015 and references therein), but more
616 recent reports (Saraiva et al., 2019a; Wählström et al., 2020; Meier et al., 2021, 2022) have
617 reaffirmed that nutrient reductions in accordance with the Baltic Sea Plan are also highly likely
618 to mitigate a substantial amount of those hypoxia increases. Repeated investigations into the
619 impact of increased discharge and higher temperatures in the Gulf of Mexico demonstrate a
620 likely expansion of hypoxic area (Justić et al. 1996; Lehrter et al., 2017; Laurent et al., 2018),
621 and additional nutrient reductions required to mitigate these impacts (Justić et al., 2003). Finally,
622 Whitney and Vlahos (2021) demonstrated a considerable erosion in oxygen gains due to nutrient
623 reductions in the presence of climate effects, reducing projected mid-century improvements by
624 14%, similar to the 9% increase in hypoxic volume reported by Irby et al. (2018) for O_2 levels $<$
625 2 mg L^{-1} . Although these studies include direct climate change impacts on coastal water bodies,
626 most support the findings here demonstrating that increases in discharge and associated nutrient
627 loadings are likely to increase Chesapeake Bay hypoxia. Overall, climate impacts on land have
628 the potential to profoundly modify biogeochemical interactions in the coastal zone and limit the
629 efficacy of nutrient reductions.

630

631 **4.3 Hypoxia Lessened by Impacts of Management Actions**

632

633 Projections of changes to watershed discharge and nutrient delivery can better inform
634 regional environmental managers tasked with managing interactions among nutrient reduction
635 strategies, climate change, and coastal hypoxia (Hood et al., 2021; BACC II, 2015; Fennel and
636 Laurent, 2018). The Chesapeake Bay results provided in this analysis demonstrate that the
637 management actions mandated to improve water quality (USEPA, 2010) will decrease hypoxia
638 by roughly 50%, approximately an order of magnitude more than projected increases due only to
639 watershed climate change (Fig. 11). Therefore, nutrient reduction strategies are very likely to
640 remain effective at reducing watershed nutrient loading and its contribution to eutrophication and
641 hypoxia over a range of possible ESM scenarios (Mastrandrea et al., 2010). Should all
642 management actions be implemented as outlined in the USEPA's Total Maximum Daily Load
643 (USEPA, 2010), it is very likely that future climate impacts on Bay watershed runoff will worsen
644 Bay hypoxia by a far smaller amount, relative to 1990s reference conditions. These findings are
645 consistent with those of Irby et al. (2018) who also examined the impacts of watershed climate
646 on Chesapeake Bay hypoxia for the mid-21st century. When evaluating the effects of watershed
647 climate impacts and management actions together, Irby et al. (2018) estimated an average AHV
648 increase of $12.8 \text{ km}^3 \text{ d}$, which is well within the range of $17.1 \pm 34.8 \text{ km}^3 \text{ d}$ reported here (Table
649 6). (Interestingly, the combined impact of all climate stressors, i.e. atmosphere, ocean, and
650 watershed, increased average AHV by $24.5 \text{ km}^3 \text{ d}$, which is also within the range of the results
651 reported here). Because climate change impacts are likely to increase total nitrogen loads,
652 implementing nutrient reductions that do not account for the detrimental effects of climate

653 change will reduce the likelihood of attaining water quality targets. Further quantifying a range
654 of future estimates of watershed discharge and nitrogen loading using regional models is critical
655 to understanding the possibilities and limitations of mitigating negative climate impacts via
656 nutrient reductions.

657 Recent findings support the hypothesis that nutrient reductions will improve water quality
658 despite projected climate impacts in both freshwater systems (Wade et al., 2022) and other
659 coastal marine systems (Whitney and Vlahos, 2021; Saraiva et al., 2019a; Bartosova et al., 2019;
660 Wählström et al., 2020; Pihlainen et al., 2020; Meier et al., 2021; Große et al., 2020; Jarvis et al.,
661 2022). In the Chesapeake Bay, reduced nutrient loading (Zhang et al., 2018; Murphy et al., 2022)
662 has already helped mitigate growing climate change pressures (Frankel et al., 2022), despite
663 rapidly increasing Bay temperatures over the past 30 years (Hinson et al., 2021). Like these prior
664 studies, our findings confirm that management actions will likely produce even greater benefits
665 to O₂ in coastal zones strongly affected by terrestrial runoff. While direct effects (e.g., air
666 temperature) are expected to increase hypoxia more so than watershed changes in Chesapeake
667 Bay (Irby et al., 2018, Ni et al., 2019), the comparatively greater impacts of management actions
668 reported here are also likely to substantially reduce the overall risk from a multitude of co-
669 occurring climatic stressors.

670

671 **4.4 Study Limitations and Future Research Directions**

672

673 Despite the plainly evident finding of nutrient reduction strategies improving water quality
674 and counteracting negative climate change watershed impacts, a number of important caveats
675 should temper this conclusion. First, the subset of scenarios that include management actions is
676 limited to a set of five ESMs statistically downscaled with a single methodology and applied to
677 one watershed model. As demonstrated in this work, this assumption may oversimplify the
678 complex relationship between climate forcings and watershed model simulations, especially
679 given that DLEM scenarios produce more change in nitrate and consequently more hypoxia than
680 Phase 6 scenarios. Management actions implemented in Phase 6 nutrient reduction scenarios
681 represent a multitude of possible methods to reduce point and nonpoint source pollution that are
682 assumed to be fully implemented with a high operational efficacy by mid-century, but the true
683 performance of best management practices operating under future hydroclimatic stressors
684 remains largely unresolved (Hanson et al., 2022). Additionally, the importance of legacy
685 nitrogen inputs to the Bay may grow over time (Ator and Denver, 2015; Chang et al., 2021), and
686 can only be properly accounted for via a long-term transient simulation that accounts for
687 changing groundwater conditions.

688 A key strength of the delta method applied here is its ability to remove the influence of
689 interannual variability, which is known to strongly influence hypoxia in the Chesapeake Bay
690 (Bever et al., 2013). However, the delta method is unable to account for the impacts of
691 unanticipated extreme events, or changing patterns of precipitation intensity, duration, and
692 frequency that produce dramatic responses in sediment washoff, scour, and consequent
693 watershed organic nitrogen export. Air temperature and precipitation were the only watershed
694 model input variables adjusted in this analysis, allowing for a more equivalent comparison
695 between downscaling approaches. Future representations of watershed change may also better
696 account for changes in runoff through the inclusion of factors like ESM-estimated relative
697 humidity that can help avoid possible unreasonable amplification of potential evapotranspiration
698 that would decrease tributary discharge (Milly and Dunne, 2011) and associated nutrient loads.

699 Although main stem Bay oxygen levels are the focus of this study, watershed impacts are
700 also likely to influence water quality in smaller scale tributaries. Differences in Chesapeake Bay
701 temperatures introduced by ESM and downscaling method have also been investigated by
702 Muhling et al. (2018), and contribute to biogeochemical variability via direct impacts of
703 atmospheric temperature on Bay warming. Incorporating different facets of these relative
704 uncertainties into projections of coastal change has also been demonstrated to affect ecological
705 outcomes like those surrounding fisheries (Reum et al., 2020; Bossier et al., 2021). Thus, the
706 impacts of these uncertainties are also very likely to affect socio-economic systems tied to
707 coastal resources. The analytical method applied here is well established within climatic and
708 terrestrial settings, so the relative dearth of coastal applications (excluding Meier et al., 2021)
709 may be more related to a consequence of computational demand or greater focus on uncertain
710 parameterizations of marine biogeochemical processes (Jarvis et al., 2022) that also play a large
711 role in potential future hypoxia outcomes.

712

713 **5 Conclusions**

714

715 Coastal ecosystems like the Chesapeake Bay that are currently and will likely continue to be
716 negatively affected by climate impacts exhibit complex responses in future scenarios,
717 demonstrating our lack of complete system understanding. While this research reaffirms the
718 importance of management actions in reducing levels of hypoxia, it also highlights the fact that
719 uncertainties in climate-impacted watershed conditions will affect estimates of Chesapeake Bay
720 O₂ levels. Additional study of uncertainty interactions within a full climate scenario (that
721 includes the impacts of changing atmospheric and oceanic conditions) will help better quantify a
722 range of hypoxia projections, among other environmental conditions within the Chesapeake Bay.
723 These results underscore the need for additional rigorous analyses of model parameterizations
724 and their contributions to model scenario uncertainty to help identify biogeochemical processes
725 that are most sensitive to climate change impacts and warrant further investigation. The
726 development of more rapid techniques to evaluate a broader range of future water quality and
727 ecological outcomes, and an inspection of their underlying assumptions, can help provide a
728 better mechanistic understanding of complex reactions to multiple climate stressors. Like
729 ongoing efforts to reduce greenhouse gas emissions and lessen the impacts of future climate
730 change globally, continuing efforts to reduce eutrophication in coastal waters will help improve
731 ecosystem resilience and the benefits derived by communities dependent on their function.
732 Indeed, nutrient reduction plans are likely to become even more essential to managers tasked
733 with preserving the health and function of rapidly evolving coastal environments and unfamiliar
734 future conditions.

735

736 **Appendix A:**

737

738 Original partitioning of organic nitrogen pools from the DLEM and Phase 6 watershed
739 models was based on fixed fractions previously described in Frankel et al. (2022). There, 80% of
740 the refractory organic nitrogen (rorN) loadings from Phase 6 were allocated to the small detritus
741 nitrogen (SDeN) pool and the remainder was applied to the refractory dissolved organic nitrogen
742 (rDON) pool in ChesROMS-ECB. More realistic changes to this partitioning of watershed rorN
743 loadings were implemented, which decreased the lability of organic nitrogen loads overall. A
744 specified threshold of rorN loadings was set at the 90th percentile of reference Phase 6 watershed
745 inputs to the estuarine model, and thresholds were also set for individual river levels of discharge
746 at the 50th and 90th percentiles of Phase 6 reference simulations. Below the 50th percentile of
747 discharge levels, 80% of the rorN inputs below the specified rorN threshold were allocated to
748 ChesROMS-ECB's SDeN pool, and the remainder were assigned to the rDON pool. Between the
749 50th and 90th percentiles of discharge events, 50% of the rorN load below the specified rorN
750 threshold was apportioned to ChesROMS-ECB's SDeN and rDON pools. At the uppermost
751 levels of discharge (greater than the 90th percentile), 5% of rorN was allocated to SDeN and 95%
752 was given to rDON within ChesROMS-ECB. For any partitioning of an organic nitrogen load,
753 regardless of the level of discharge, rorN loading above this cutoff was allocated to ChesROMS-
754 ECB's rDON pool. The rorN load below this threshold was allocated according to the
755 fractionations described above. Changes to Phase 6 watershed loadings were mapped to
756 equivalent DLEM watershed input variables, following the methodology of Frankel et al. (2022).

757

758 **Table A1. Acronyms and Abbreviations**

AHV	Annual Hypoxic Volume
BCSD	Bias-Correction and Spatial Disaggregation
CBP	Chesapeake Bay Program
ChesROMS-ECB	Chesapeake Regional Ocean Modeling System – Estuarine Carbon and Biogeochemistry
CMIP	Coupled Model Intercomparison Project
DIN	Dissolved Inorganic Nitrogen
DLEM	Dynamic Land Ecosystem Model
DON	Dissolved Organic Nitrogen
DSC	Downscaling Methodology
ESM	Earth System Model
KKZ	Katsavounidis-Kuo-Zhang (Katsavounidis et al., 1994)
MACA	Multivariate Adapted Constructed Analogs
Phase 6	Phase 6 Watershed Model
RCP	Representative Concentration Pathway
WSM	Watershed Model

759

760

761

762 **Appendix B:**

763
 764 An example calculation of the methodology used to calculate uncertainty for a single
 765 component of the total uncertainty is provided below. Average annual changes in hypoxic
 766 volume (km³ d) are shown in the table below for the Multi-Factor experiment. Values of hypoxic
 767 volume are rounded to the tenth decimal place in Tables 1-3, but the rounding is not carried
 768 through all calculations.

769

ESM	P6 MACA	P6 BCSD	DLEM MACA	DLEM BCSD
KKZ1	-34.3	34.6	53.4	-2.0
KKZ2	-18.8	57.7	7.2	-12.5
KKZ3	24.8	23.8	139.2	71.8
KKZ4	-10.7	-32.3	88.0	8.6
KKZ5	64.7	93.7	24.3	94.3

770
 771 For the first calculation, a subset of two ESMs is selected so that the number of values is
 772 balanced among ESMs, downscaling methods, and watershed models. This process will be
 773 repeated for each possible combination of ESMs, ten in total {(1,2), (1,3), (1,4), ..., (4, 5)}.

774

ESM	P6 MACA	P6 BCSD	DLEM MACA	DLEM BCSD
KKZ1	-34.3	34.6	53.4	-2.0
KKZ2	-18.8	57.7	7.2	-12.5

775
 776 For simplicity, the above table can be rearranged to that shown below. Additionally, the format
 777 of the table below and the following equations largely mirror the format of Ohn et al. (2021).

Stage 1 (E)	Stage 2 (D)	Stage 3 (W)	Y _x
X _{1,1}	X _{2,1}	X _{3,1}	-34.3
		X _{3,2}	53.4
	X _{2,2}	X _{3,1}	34.6
		X _{3,2}	-2.0
X _{1,2}	X _{2,1}	X _{3,1}	-18.8
		X _{3,2}	7.2
	X _{2,2}	X _{3,1}	57.7
		X _{3,2}	-12.5

778
 779 First, the total variance of this subset ($U_{\{1,2,3\}}^{cumul}$) is calculated, with the subscripts of each
 780 individual factor (ESM=1, DSC=2, WSM=3) denoted:

781

$$U_{\{1,2,3\}}^{cumul} = \frac{1}{N} \sum_i^N (X_i - \bar{X})^2 = 1025.1$$

782 Following this, the cumulative uncertainty due to the choice of downscaling method and
 783 watershed model ($U_{\{2,3\}}^{cumul}$) is calculated by selecting all values produced individual ESMs:

784

$$Y_{\{1,2\}}(x_{3,1}) = \{-34.3, 34.6, -18.8, 57.7\}$$

785

$$Y_{\{1,2\}}(x_{3,2}) = \{53.4, -2.0, 7.2, -12.5\}$$

786
$$U_{\{1,2\}}^{cumul} = \frac{1}{2}(U_{\{1,2\}}^{cumul}(x_{3,1}) + U_{\{1,2\}}^{cumul}(x_{3,1})) = \frac{1}{2}(1417.0 + 631.7) = 1024.3$$

787

788 Similar variance calculations are completed for the uncertainty of the first stage alone ($U_{\{1\}}^{cumul}$),
789 where the choice of ESM is the only constant:

790
$$Y_{\{1\}}(x_{2,1}, x_{3,1}) = \{-34.3, -18.8\}$$

791
$$Y_{\{1\}}(x_{2,1}, x_{3,2}) = \{53.4, 7.2\}$$

792
$$Y_{\{1\}}(x_{2,2}, x_{3,1}) = \{34.6, 57.7\}$$

793
$$Y_{\{1\}}(x_{2,2}, x_{3,2}) = \{-2.0, -12.5\}$$

794

795 Combining these values to calculate the uncertainty of the first stage alone (ESM) yields:

796
$$U_{\{1\}}^{cumul} = \frac{1}{4} \sum_{i=1}^2 \sum_{j=1}^2 (Y_{\{1\}}(x_{2,i}, x_{3,j})) = \frac{1}{4}(60.1 + 533.6 + 133.4 + 52.6) \approx 188.2$$

797

798 Applying similar calculations produces the following values necessary to compute total
799 uncertainty for all stages:

800
$$U_{\{1,2,3\}}^{cumul} = 1025.1$$

801
$$U_{\{1,2\}}^{cumul} = 1024.3$$

802
$$U_{\{2,3\}}^{cumul} = 1019.9$$

803
$$U_{\{1,3\}}^{cumul} = 947.7$$

804
$$U_{\{1\}}^{cumul} = 188.2$$

805
$$U_{\{2\}}^{cumul} = 877.7$$

806
$$U_{\{3\}}^{cumul} = 913.4$$

807

808 Next, the uncertainty of the first stage is calculated by subtracting the uncertainties from other
809 stages as follows:

810
$$U_{\{1,2,3\},1}^{cumul} = U_{\{1,2,3\}}^{cumul} - U_{\{2,3\}}^{cumul} = 5.1$$

811
$$U_{\{1,2\},1}^{cumul} = U_{\{1,2\}}^{cumul} - U_{\{2\}}^{cumul} = 146.6$$

812
$$U_{\{1,3\},1}^{cumul} = U_{\{1,3\}}^{cumul} - U_{\{3\}}^{cumul} = 34.4$$

813
$$U_{\{1\},1}^{cumul} = 188.2$$

814

815 The combined value of cumulative uncertainty for the first stage (ESM) can now be calculated:

816
$$\frac{1}{3}(U_{\{1,2,3\},1}^{cumul} + \frac{1}{2}U_{\{1,2\},1}^{cumul} + \frac{1}{2}U_{\{1,3\},1}^{cumul} + U_{\{1\},1}^{cumul}) = \frac{1}{3}(5.1 + 73.3 + 17.2 + 188.2) = 94.6$$

817

818 Applying the same computational steps results in cumulative uncertainties for stages 2
819 (Downscaling Method) and 3 (Watershed Model) of 475.5 and 480.5, respectively. These values
820 correspond to relative uncertainties for ESM, Downscaling Method, and Watershed Model of
821 9%, 45%, and 46%, respectively. This procedure is then repeated for all other combinations of
822 two ESMs $\{(1,3), (1,4), (1,5), \dots, (4,5)\}$, after which the percentage values are averaged to
823 produce the estimates reported in our results.

824 **Competing Interests:** The authors declare that they have no conflict of interest.

825

826 **Author contribution:** MF, RN, HT, and GS were responsible for project conceptualization and
827 funding acquisition. MH, ZB, and GB were responsible for data curation used in the
828 experiments. KH and MF planned the model experiments; KH, MF, and PS are responsible for
829 the methodology (model creation). KH conducted the investigation and formal analysis, and
830 created software and visualizations of results; KH wrote the original manuscript draft; MF, RN,
831 MH, ZB, GB, PS, HT, and GS reviewed and edited the manuscript.

832

833 **Acknowledgements:** This paper is the result of research funded by the National Oceanic and
834 Atmospheric Administration's National Centers for Coastal Ocean Science under award
835 NA16NOS4780207 to the Virginia Institute of Marine Science. Additional funding support was
836 provided by the VIMS Academic Studies Office. Feedback from principal investigators, team
837 members, and the Management Transition and Advisory Group of the Chesapeake Hypoxia
838 Analysis & Modeling Program (CHAMP) benefited this research. The authors acknowledge
839 William & Mary Research Computing for providing computational resources and/or technical
840 support that have contributed to the results reported within this paper

841 (<https://www.wm.edu/it/rc>). The authors also acknowledge the World Climate Research
842 Programme's Working Group on Coupled Modelling, which is responsible for CMIP, and we
843 thank the climate modeling groups (listed in Table S3 of this paper) for producing and making
844 available their model output. For CMIP, the U.S. Department of Energy's Program for Climate
845 Model Diagnosis and Intercomparison provides coordinating support and led development of
846 software infrastructure in partnership with the Global Organization for Earth System Science
847 Portals. The model results used in the manuscript are permanently archived at the W&M
848 ScholarWorks data repository associated with this article and are available for free download
849 (<https://doi.org/xxxx>). Finally, the authors would like to thank the anonymous reviewer and Bo
850 Gustafsson for their helpful and insightful comments that helped improve the manuscript.

851 **References**

- 852
- 853 Abatzoglou, J. T., & Brown, T. J.: A comparison of statistical downscaling methods suited for
854 wildfire applications, *Int. J. Climatol.*, 32, 5, 772–780, <https://doi.org/10.1002/joc.2312>,
855 2012.
- 856 Anandhi, A., Frei, A., Pierson, D. C., Schneiderman, E. M., Zion, M. S., Lounsbury, D., &
857 Matonse, A. H.: Examination of change factor methodologies for climate change impact
858 assessment, *Water Resour. Res.*, 47, 3, 1–10, <https://doi.org/10.1029/2010WR009104>, 2011.
- 859 Ator, S.W., and Denver, J.M.: Understanding nutrients in the Chesapeake Bay watershed and
860 implications for management and restoration—the Eastern Shore (ver. 1.2, June 2015): U.S.
861 Geological Survey Circular 1406, 72 p., <http://dx.doi.org/10.3133/cir1406>, 2015.
- 862 Ator, S., Schwarz, G. E., Sekellick, A. J., & Bhatt, G.: Predicting Near-Term Effects of Climate
863 Change on Nitrogen Transport to Chesapeake Bay, *J. Am. Water Resour. Assoc.*, 58, 4, 578–
864 596, <https://doi.org/10.1111/1752-1688.13017>, 2022.
- 865 BACC II Author Team: Second Assessment of Climate Change for the Baltic Sea Basin, in:
866 Regional Climate Studies, Springer International Publishing, Cham,
867 <https://doi.org/10.1007/978-3-319-16006-1>, 2015.
- 868 Bartosova, A., Capell, R., Olesen, J. E., Jabloun, M., Refsgaard, J. C., Donnelly, C., Hyytiäinen,
869 K., Pihlainen, S., Zandersen, M., and Arheimer, B.: Future socioeconomic conditions may
870 have a larger impact than climate change on nutrient loads to the Baltic Sea, *Ambio*, 48,
871 1325–1336, <https://doi.org/10.1007/s13280-019-01243-5>, 2019.
- 872 Basenback, N., Testa, J. M., and Shen, C.: Interactions of Warming and Altered Nutrient Load
873 Timing on the Phenology of Oxygen Dynamics in Chesapeake Bay, *J. Am. Water Resour.*
874 *Assoc.*, 1752–1688.13101, <https://doi.org/10.1111/1752-1688.13101>, 2022.
- 875 Bevacqua, E., Shepherd, T. G., Watson, P. A. G., Sparrow, S., Wallom, D., & Mitchell, D.:
876 Larger Spatial Footprint of Wintertime Total Precipitation Extremes in a Warmer Climate,
877 *Geophys. Res. Lett.*, 48, 8, <https://doi.org/10.1029/2020GL091990>, 2021.
- 878 Bever, A. J., Friedrichs, M. A. M., Friedrichs, C. T., Scully, M. E., & Lanerolle, L. W. J.:
879 Combining observations and numerical model results to improve estimates of hypoxic
880 volume within the Chesapeake Bay, USA, *J. Geophys. Res. Ocean.*, 118, 10, 4924–4944,
881 <https://doi.org/10.1002/jgrc.20331>, 2013.
- 882 Bever, A. J., Friedrichs, M. A. M., Friedrichs, C. T., & Scully, M. E.: Estimating Hypoxic
883 Volume in the Chesapeake Bay Using Two Continuously Sampled Oxygen Profiles, *J.*
884 *Geophys. Res. Ocean.*, 123, 9, 6392–6407, <https://doi.org/10.1029/2018JC014129>, 2018.
- 885 Bever, A. J., Friedrichs, M. A. M., & St-Laurent, P.: Real-time environmental forecasts of the
886 Chesapeake Bay: Model setup, improvements, and online visualization, *Environ. Model.*
887 *Softw.*, 140, March, <https://doi.org/10.1016/j.envsoft.2021.105036>, 2021.
- 888 Bosshard, T., Carambia, M., Goergen, K., Kotlarski, S., Krahe, P., Zappa, M., & Schär, C.:
889 Quantifying uncertainty sources in an ensemble of hydrological climate-impact projections,
890 *Water Resour. Res.*, 49, 3, 1523–1536, <https://doi.org/10.1029/2011WR011533>, 2013.
- 891 Bossier, S., Nielsen, J. R., Almroth-Rosell, E., Höglund, A., Bastardie, F., Neuenfeldt, S.,
892 Wählström, I., & Christensen, A.: Integrated ecosystem impacts of climate change and
893 eutrophication on main Baltic fishery resources, *Ecol. Modell.*, 453, May,
894 <https://doi.org/10.1016/j.ecolmodel.2021.109609>, 2021.
- 895 Breitburg, D., Levin, L. A., Oschlies, A., Grégoire, M., Chavez, F. P., Conley, D. J., Garçon, V.,
896 Gilbert, D., Gutiérrez, D., Isensee, K., Jacinto, G. S., Limburg, K. E., Montes, I., Naqvi, S.

897 W. A., Pitcher, G. C., Rabalais, N. N., Roman, M. R., Rose, K. A., Seibel, B. A., ... Zhang,
898 J.: Declining oxygen in the global ocean and coastal waters, *Science* (80-.), 359, 6371,
899 <https://doi.org/10.1126/science.aam7240>, 2018.

900 C3S (Copernicus Climate Change Service).: “ERA5: Fifth Generation of ECMWF Atmospheric
901 Reanalyses of the Global Climate.” Copernicus Climate Change Service Climate Data Store
902 (CDS). <https://cds.climate.copernicus.eu/cdsapp#!/home>, 2017.

903 Cai, X., Shen, J., Zhang, Y. J., Qin, Q., Wang, Z., & Wang, H.: Impacts of Sea-Level Rise on
904 Hypoxia and Phytoplankton Production in Chesapeake Bay: Model Prediction and
905 Assessment, *J. Am. Water Resour. Assoc.*, 1–18, <https://doi.org/10.1111/1752-1688.12921>,
906 2021.

907 Carter, T.R., Parry, M.L., Nishioka, S. and Harasawa, H., 1994. Technical Guidelines for
908 Assessing Climate Change Impacts and Adaptations. Intergovernmental Panel on Climate
909 Change Working Group II. University College London and Center for Global Environmental
910 Research, Japan. 60 pp.

911 Chang, S. Y., Zhang, Q., Byrnes, D. K., Basu, N. B., & van Meter, K. J.: Chesapeake legacies:
912 The importance of legacy nitrogen to improving Chesapeake Bay water quality, *Environ.*
913 *Res. Lett.*, 16, 8, <https://doi.org/10.1088/1748-9326/ac0d7b>, 2021.

914 Chesapeake Bay Program DataHub: <http://data.chesapeakebay.net/WaterQuality>, last access: 18
915 April 2022.

916 Chesapeake Bay Program. Chesapeake Assessment and Scenario Tool (CAST) Version 2019.
917 Chesapeake Bay Program Office, <https://cast.chesapeakebay.net/>, 2020.

918 Da, F., Friedrichs, M. A. M., St-Laurent, P., Shadwick, E. H., Najjar, R. G., & Hinson, K. E.:
919 Mechanisms Driving Decadal Changes in the Carbonate System of a Coastal Plain Estuary, *J.*
920 *Geophys. Res. Ocean.*, 126, 6, 1–23, <https://doi.org/10.1029/2021JC017239>, 2021.

921 Dussin, R., Curchitser, E. N., Stock, C. A., & Van Oostende, N.: Biogeochemical drivers of
922 changing hypoxia in the California Current Ecosystem, *Deep. Res. Part II Top. Stud.*
923 *Oceanogr.*, 169–170, May, 104590, <https://doi.org/10.1016/j.dsr2.2019.05.013>, 2019.

924 Easton, Z., Scavia, D., Alexander, R., Band, L., Boomer, K., Kleinman, P., Martin, J., Miller, A.,
925 Pizzuto, J., Smith, D., Welty, C., Easton, Z., Scavia, D., Alexander, R., Band, L., Boomer,
926 K., Kleinman, P., Martin, J., & Miller, A.: Scientific and Technical Advisory Committee
927 Chesapeake Bay Watershed Model Phase 6 Review STAC Review Report (Vol. 47, Issue
928 September), 2017.

929 Feng, Y., Friedrichs, M. A. M., Wilkin, J., Tian, H., Yang, Q., Hofmann, E. E., Wiggert, J. D., &
930 Hood, R. R.: Chesapeake Bay nitrogen fluxes derived from a land- estuarine ocean
931 biogeochemical modeling system: Model description, evaluation, and nitrogen budgets, *J.*
932 *Geophys. Res. Biogeosciences*, 120, 1666–1695, <https://doi.org/10.1002/2017JG003800>,
933 2015.

934 Fennel, K., & Laurent, A.: N and P as ultimate and proximate limiting nutrients in the northern
935 Gulf of Mexico: Implications for hypoxia reduction strategies, *Biogeosciences*, 15, 10, 3121–
936 3131, <https://doi.org/10.5194/bg-15-3121-2018>, 2018.

937 Fennel, K., Gehlen, M., Brasseur, P., Brown, C. W., Ciavatta, S., Cossarini, G., Crise, A.,
938 Edwards, C. A., Ford, D., Friedrichs, M. A. M., Gregoire, M., Jones, E., Kim, H.-C.,
939 Lamouroux, J., Murtugudde, R., Perruche, C., and the GODAE OceanView Marine
940 Ecosystem Analysis and Prediction Task Team: Advancing Marine Biogeochemical and
941 Ecosystem Reanalyses and Forecasts as Tools for Monitoring and Managing Ecosystem
942 Health, *Front. Mar. Sci.*, 6, <https://doi.org/10.3389/fmars.2019.00089>, 2019.

943 Frankel, L. T., Friedrichs, M. A. M., St-Laurent, P., Bever, A. J., Lipcius, R. N., Bhatt, G., &
944 Shenk, G. W.: Nitrogen reductions have decreased hypoxia in the Chesapeake Bay: Evidence
945 from empirical and numerical modeling, *Sci. Total Environ.*, 814,
946 <https://doi.org/10.1016/j.scitotenv.2021.152722>, 2022.

947 Gilbert, D., Rabalais, N. N., Díaz, R. J., & Zhang, J.: Evidence for greater oxygen decline rates
948 in the coastal ocean than in the open ocean, *Biogeosciences*, 7, 7, 2283–2296,
949 <https://doi.org/10.5194/bg-7-2283-2010>, 2010.

950 Große, F., Fennel, K., Zhang, H., & Laurent, A.: Quantifying the contributions of riverine vs.
951 oceanic nitrogen to hypoxia in the East China Sea, *Biogeosciences*, 17, 10, 2701–2714,
952 <https://doi.org/10.5194/bg-17-2701-2020>, 2020.

953 Gudmundsson, L., Boulange, J., Do, H. X., Gosling, S. N., Grillakis, M. G., Koutroulis, A. G.,
954 Leonard, M., Liu, J., Schmied, H. M., Papadimitriou, L., Pokhrel, Y., Seneviratne, S. I.,
955 Satoh, Y., Thiery, W., Westra, S., Zhang, X., & Zhao, F.: Globally observed trends in mean
956 and extreme river flow attributed to climate change, *Science*, 371, 6534, 1159–1162,
957 <https://doi.org/10.1126/science.aba3996>, 2021.

958 Hagy, J. D., Boynton, W. R., Keefe, C. W., & Wood, K. V.: Hypoxia in Chesapeake Bay, 1950-
959 2001: Long-term change in relation to nutrient loading and river flow, *Estuaries*, 27, 4, 634–
960 658, <https://doi.org/10.1007/BF02907650>, 2004.

961 Hanson, J., E. Bock, B. Asfaw, and Z.M. Easton.: A systematic review of Chesapeake Bay
962 climate change impacts and uncertainty: watershed processes, pollutant delivery and BMP
963 performance. CBP/TRS-330-22. Available at <https://bit.ly/BMP-CC-synth>, 2022.

964 Harding, L. W., Mallonee, M. E., & Perry, E. S.: Toward a predictive understanding of primary
965 productivity in a temperate, partially stratified estuary, *Estuar. Coast. Shelf Sci.*, 55, 3, 437–
966 463, <https://doi.org/10.1006/ecss.2001.0917>, 2002.

967 Hawkins, E., & Sutton, R.: The potential to narrow uncertainty in regional climate predictions,
968 *Bull. Am. Meteorol. Soc.*, 90, 8, 1095–1107, <https://doi.org/10.1175/2009BAMS2607.1>,
969 2009.

970 Hein, B., Viergutz, C., Wyrwa, J., Kirchesch, V., & Schöl, A.: Impacts of climate change on the
971 water quality of the Elbe Estuary (Germany), *J. Appl. Water Eng. Res.*, 6, 1, 28–39,
972 <https://doi.org/10.1080/23249676.2016.1209438>, 2018.

973 Hinson, K. E., Friedrichs, M. A. M., St-Laurent, P., Da, F., & Najjar, R. G.: Extent and Causes of
974 Chesapeake Bay Warming, *J. Am. Water Resour. Assoc.*, 1–21,
975 <https://doi.org/10.1111/1752-1688.12916>, 2021.

976 Hirsch, R. M., Moyer, D. L., & Archfield, S. A.: Weighted regressions on time, discharge, and
977 season (WRTDS), with an application to Chesapeake Bay river inputs, *J. Am. Water Resour.*
978 *Assoc.*, 46, 5, 857–880, <https://doi.org/10.1111/j.1752-1688.2010.00482.x>, 2010.

979 Hong, B., Liu, Z., Shen, J., Wu, H., Gong, W., Xu, H., & Wang, D.: Potential physical impacts
980 of sea-level rise on the Pearl River Estuary, China, *J. Mar. Syst.*, 201,
981 <https://doi.org/10.1016/j.jmarsys.2019.103245>, 2020.

982 Hood, R. R., Shenk, G. W., Dixon, R. L., Smith, S. M. C., Ball, W. P., Bash, J. O., Batiuk, R.,
983 Boomer, K., Brady, D. C., Cerco, C., Claggett, P., de Mutsert, K., Easton, Z. M., Elmore, A.
984 J., Friedrichs, M. A. M., Harris, L. A., Ihde, T. F., Lacher, L., Li, L., ... Zhang, Y. J.: The
985 Chesapeake Bay program modeling system: Overview and recommendations for future
986 development, *Ecol. Modell.*, 456, July, <https://doi.org/10.1016/j.ecolmodel.2021.109635>,
987 2021.

- 988 Howarth, R. W., Swaney, D. P., Boyer, E. W., Marino, R., Jaworski, N., & Goodale, C.: The
989 influence of climate on average nitrogen export from large watersheds in the Northeastern
990 United States, *Biogeochemistry*, 79, 1–2, 163–186, [https://doi.org/10.1007/s10533-006-](https://doi.org/10.1007/s10533-006-9010-1)
991 9010-1, 2006.
- 992 Huang, H., Patricola, C. M., Winter, J. M., Osterberg, E. C., & Mankin, J. S.: Rise in Northeast
993 US extreme precipitation caused by Atlantic variability and climate change, *Weather Clim.*
994 *Extrem.*, 33, January, <https://doi.org/10.1016/j.wace.2021.100351>, 2021.
- 995 IPCC, 2013: *Climate Change 2013: The Physical Science Basis. Contribution of Working Group*
996 *I to the Fifth Assessment Report of the Intergovernmental Panel on Climate Change*
997 [Stocker, T.F., D. Qin, G.-K. Plattner, M. Tignor, S.K. Allen, J. Boschung, A. Nauels, Y.
998 Xia, V. Bex and P.M. Midgley (eds.)]. Cambridge University Press, Cambridge, United
999 Kingdom and New York, NY, USA, 1535 pp.
- 1000 Irby, I. D., Friedrichs, M. A. M., Da, F., & Hinson, K. E.: The competing impacts of climate
1001 change and nutrient reductions on dissolved oxygen in Chesapeake Bay, *Biogeosciences*, 15,
1002 9, 2649–2668, <https://doi.org/10.5194/bg-15-2649-2018>, 2018.
- 1003 Irby, I. D., Friedrichs, M. A. M., Friedrichs, C. T., Bever, A. J., Hood, R. R., Lanerolle, L. W. J.,
1004 Scully, M. E., Sellner, K., Shen, J., Testa, J., Li, M., Wang, H., Wang, P., Linker, L., & Xia,
1005 M.: Challenges associated with modeling low-oxygen waters in Chesapeake Bay: A multiple
1006 model comparison, *Biogeosciences*, 13, 7, 2011–2028, [https://doi.org/10.5194/bgd-12-](https://doi.org/10.5194/bgd-12-20361-2015)
1007 20361-2015, 2016.
- 1008 Jarvis, B. M., Pauer, J. J., Melendez, W., Wan, Y., Lehrter, J. C., Lowe, L. L., & Simmons, C.
1009 W.: Inter-model comparison of simulated Gulf of Mexico hypoxia in response to reduced
1010 nutrient loads: Effects of phytoplankton and organic matter parameterization, *Environ.*
1011 *Model. Softw.*, 151, 105365, <https://doi.org/10.1016/j.envsoft.2022.105365>, 2022.
- 1012 Justić, D., Bierman Jr, V. J., Scavia, D., & Hetland, R. D.: Forecasting Gulf’s Hypoxia : The
1013 Next 50 Years ? Forecasting Gulf’s Hypoxia: The Next 50 Years ?, *Estuaries and Coasts*, 30,
1014 5, 791–801, <https://doi.org/10.1007/BF02841334>, 2007.
- 1015 Justić, D., Rabalais, N. N., & Turner, R. E.: Effects of climate change on hypoxia in coastal
1016 waters: A doubled CO2 scenario for the northern Gulf of Mexico, *Limnol. Oceanogr.*, 41, 5,
1017 992–1003, <https://doi.org/10.4319/lo.1996.41.5.0992>, 1996.
- 1018 Justić, D., Rabalais, N. N., & Turner, R. E.: Simulated responses of the Gulf of Mexico hypoxia
1019 to variations in climate and anthropogenic nutrient loading, *J. Mar. Syst.*, 42, 3–4, 115–126,
1020 [https://doi.org/10.1016/S0924-7963\(03\)00070-8](https://doi.org/10.1016/S0924-7963(03)00070-8), 2003.
- 1021 Katsavounidis, I., Kuo, C. C. J., & Zhang, Z.: A New Initialization Technique for Generalized
1022 Lloyd Iteration, *IEEE Signal Process. Lett.*, 1, 10, 144–146,
1023 <https://doi.org/10.1109/97.329844>, 1994.
- 1024 Kemp, W. M., Boynton, W. R., Adolf, J. E., Boesch, D. F., Boicourt, W. C., Brush, G.,
1025 Cornwell, J. C., Fisher, T. R., Glibert, P. M., Hagy, J. D., Harding, L. W., Houde, E. D.,
1026 Kimmel, D. G., Miller, W. D., Newell, R. I. E., Roman, M. R., Smith, E. M., & Stevenson, J.
1027 C.: Eutrophication of Chesapeake Bay: Historical trends and ecological interactions, *Mar.*
1028 *Ecol. Prog. Ser.*, 303, 1–29, <https://doi.org/10.3354/meps303001>, 2005.
- 1029 Lachkar, Z., Lévy, M., & Smith, K. S.: Strong Intensification of the Arabian Sea Oxygen
1030 Minimum Zone in Response to Arabian Gulf Warming, *Geophys. Res. Lett.*, 46, 10, 5420–
1031 5429, <https://doi.org/10.1029/2018GL081631>, 2019.
- 1032 Lajaunie-Salla, K., Sottolichio, A., Schmidt, S., Litrico, X., Binet, G., & Abril, G.: Future
1033 intensification of summer hypoxia in the tidal Garonne River (SW France) simulated by a

1034 coupled hydro sedimentary-biogeochemical model, *Environ. Sci. Pollut. Res.*, 25, 32, 31957–
1035 31970, <https://doi.org/10.1007/s11356-018-3035-6>, 2018.

1036 Laurent, A., Fennel, K., Ko, D. S., & Lehrter, J.: Climate change projected to exacerbate impacts
1037 of coastal Eutrophication in the Northern Gulf of Mexico, *J. Geophys. Res. Ocean.*, 123, 5,
1038 3408–3426, <https://doi.org/10.1002/2017JC013583>, 2018.

1039 Lee, M., Shevliakova, E., Malyshev, S., Milly, P. C. D., & Jaffé, Peter, R.: Climate variability
1040 and extremes, interacting with nitrogen storage, amplify eutrophication risk, *Geophys. Res.
1041 Lett.*, 43, 7520–7528, <https://doi.org/10.1002/2016GL069254>, 2016.

1042 Lehrter, J. C., Ko, D. S., Lowe, L. L., & Penta, B.: Predicted Effects of Climate Change on
1043 Northern Gulf of Mexico Hypoxia, In D. Justić, K. A. Rose, R. D. Hetland, & K. Fennel
1044 (Eds.), *Modeling Coastal Hypoxia: Numerical Simulations of Patterns, Controls and Effects
1045 of Dissolved Oxygen Dynamics* (pp. 173–214) Springer https://doi.org/10.1007/978-3-319-54571-4_8, 2017.

1047 Lomas, M. W., Glibert, P. M., Shiah, F. K., & Smith, E. M.: Microbial processes and
1048 temperature in Chesapeake Bay: Current relationships and potential impacts of regional
1049 warming, *Glob. Chang. Biol.*, 8, 1, 51–70, <https://doi.org/10.1046/j.1365-2486.2002.00454.x>,
1050 2002.

1051 MACAv2-METDATA: [https://data.nal.usda.gov/dataset/climate-data-rpa-2020-assessment-
1052 macav2-metdata-historical-modeled-1950-2005-and-future-2006-2099-projections-
1053 conterminous-united-states-124-degree-grid-scale](https://data.nal.usda.gov/dataset/climate-data-rpa-2020-assessment-macav2-metdata-historical-modeled-1950-2005-and-future-2006-2099-projections-conterminous-united-states-124-degree-grid-scale), last access: 25 April 2018.

1054 Madakumbura, G. D., Goldenson, N., & Hall, A.: Over Global Land Areas Seen in Multiple
1055 Observational Datasets, *Nat. Commun.* <http://dx.doi.org/10.1038/s41467-021-24262-x> 2021.

1056 Mastrandrea, M.D., Field, C.B., Stocker, T.F., Edenhofer O., Ebi, K.L., Frame, D.J., Held H.,
1057 Kriegler, E., Mach, K.J., Matschoss, P.R., Plattner, G.-K., Yohe, G.W., & Zwiers, F.W.:
1058 Guidance Note for Lead Authors of the IPCC Fifth Assessment Report on Consistent
1059 Treatment of Uncertainties. Intergovernmental Panel on Climate Change (IPCC). Available
1060 at <http://www.ipcc.ch>, 2010.

1061 Meier, H. E. M., Andersson, H. C., Eilola, K., Gustafsson, B. G., Kuznetsov, I., Mller-Karulis,
1062 B., Neumann, T., & Savchuk, O. P.: Hypoxia in future climates: A model ensemble study for
1063 the Baltic Sea, *Geophys. Res. Lett.*, 38, 24, 1–6, <https://doi.org/10.1029/2011GL049929>,
1064 2011a.

1065 Meier, H. E. M., Dieterich, C., & Gröger, M.: Natural variability is a large source of uncertainty
1066 in future projections of hypoxia in the Baltic Sea, *Commun. Earth Environ.*, 2, 1,
1067 <https://doi.org/10.1038/s43247-021-00115-9>, 2021.

1068 Meier, H. E. M., Dieterich, C., Gröger, M., Duthel, C., Börgel, F., Safonova, K., Christensen, O.
1069 B., & Kjellström, E.: Oceanographic regional climate projections for the Baltic Sea until
1070 2100, *Earth Syst. Dyn.*, 13, 159–199, <https://doi.org/10.5194/esd-13-159-2022>, 2022.

1071 Meier, H. E. M., Edman, M., Eilola, K., Placke, M., Neumann, T., Andersson, H. C.,
1072 Brunnabend, S. E., Dieterich, C., Frauen, C., Friedland, R., Gröger, M., Gustafsson, B. G.,
1073 Gustafsson, E., Isaev, A., Kniebusch, M., Kuznetsov, I., Müller-Karulis, B., Naumann, M.,
1074 Omstedt, A., ... Savchuk, O. P.: Assessment of uncertainties in scenario simulations of
1075 biogeochemical cycles in the Baltic Sea, *Front. Mar. Sci.*, 6, MAR,
1076 <https://doi.org/10.3389/fmars.2019.00046>, 2019.

1077 Meier, H. E. M., Eilola, K., & Almroth, E.: Climate-related changes in marine ecosystems
1078 simulated with a 3-dimensional coupled physical-biogeochemical model of the Baltic Sea,
1079 *Clim. Res.*, 48, 1, 31–55, <https://doi.org/10.3354/cr00968>, 2011b.

1080 Meire, L., Soetaert, K. E. R., & Meysman, F. J. R.: Impact of global change on coastal oxygen
1081 dynamics and risk of hypoxia, *Biogeosciences*, 10, 4, 2633–2653, [https://doi.org/10.5194/bg-](https://doi.org/10.5194/bg-10-2633-2013)
1082 10-2633-2013, 2013.

1083 Milly, P. C. D., & Dunne, K. A.: On the hydrologic adjustment of climate-model projections:
1084 The potential pitfall of potential evapotranspiration, *Earth Interact.*, 15, 1, 1–14,
1085 <https://doi.org/10.1175/2010EI363.1>, 2011.

1086 Muhling, B. A., Gaitán, C. F., Stock, C. A., Saba, V. S., Tommasi, D., & Dixon, K. W.: Potential
1087 Salinity and Temperature Futures for the Chesapeake Bay Using a Statistical Downscaling
1088 Spatial Disaggregation Framework, *Estuaries and Coasts*, 41, 2, 349–372,
1089 <https://doi.org/10.1007/s12237-017-0280-8>, 2018.

1090 Murphy, R. R., Keisman, J., Harcum, J., Karrh, R. R., Lane, M., Perry, E. S., & Zhang, Q.:
1091 Nutrient Improvements in Chesapeake Bay: Direct Effect of Load Reductions and
1092 Implications for Coastal Management, *Environ. Sci. Technol.*, 56, 1, 260–270,
1093 <https://doi.org/10.1021/acs.est.1c05388>, 2022.

1094 Najjar, R. G., Pyke, C. R., Adams, M. B., Breitburg, D., Hershner, C., Kemp, M., Howarth, R.,
1095 Mulholland, M. R., Paolisso, M., Secor, D., Sellner, K., Wardrop, D., & Wood, R.: Potential
1096 climate-change impacts on the Chesapeake Bay, *Estuar. Coast. Shelf Sci.*, 86, 1, 1–20,
1097 <https://doi.org/10.1016/j.ecss.2009.09.026>, 2010.

1098 Nash, J. E., & Sutcliffe, J. V.: River Flow Forecasting through Conceptual Models Part I - A
1099 Discussion of Principles*, *J. Hydrol.*, 10, 282–290, 1970.

1100 Neumann, T., Eilola, K., Gustafsson, B., Müller-Karulis, B., Kuznetsov, I., Meier, H. E. M., &
1101 Savchuk, O. P.: Extremes of temperature, oxygen and blooms in the baltic sea in a changing
1102 climate, *Ambio*, 41, 6, 574–585, <https://doi.org/10.1007/s13280-012-0321-2>, 2012.

1103 Ni, W., Li, M., Ross, A. C., & Najjar, R. G.: Large Projected Decline in Dissolved Oxygen in a
1104 Eutrophic Estuary Due to Climate Change, *J. Geophys. Res. Ocean.*, 124, 11, 8271–8289,
1105 <https://doi.org/10.1029/2019JC015274>, 2019.

1106 Northrop, P. J., & Chandler, R. E.: Quantifying sources of uncertainty in projections of future
1107 climate, *J. Clim.*, 27, 23, 8793–8808, <https://doi.org/10.1175/JCLI-D-14-00265.1>, 2014.

1108 Officer, C. B., Biggs, R. B., Taft, J. L., Cronin, L. E., Tyler, M. A., & Boynton, W. R.:
1109 Chesapeake Bay anoxia: Origin, development, and significance, *Science*, 223, 4631, 22–27,
1110 <https://doi.org/10.1126/science.223.4631.22>, 1984.

1111 Ohn, I., Kim, S., Seo, S. B., Kim, Y. O., & Kim, Y.: Model-wise uncertainty decomposition in
1112 multi-model ensemble hydrological projections, *Stoch. Environ. Res. Risk Assess.*, 35, 12,
1113 2549–2565, <https://doi.org/10.1007/s00477-021-02039-4>, 2021.

1114 Olson, M.: Guide to Using Chesapeake Bay Program Water Quality Monitoring Data, edited by
1115 M. Mallonee and M.E. Ley. Annapolis, MD: Chesapeake Bay Program, 2012.

1116 Pan, S., Bian, Z., Tian, H., Yao, Y., Najjar, R. G., Friedrichs, M. A. M., Hofmann, E. E., Xu, R.,
1117 & Zhang, B.: Impacts of Multiple Environmental Changes on Long-Term Nitrogen Loading
1118 From the Chesapeake Bay Watershed, *J. Geophys. Res. Biogeosciences*, 126, 5,
1119 <https://doi.org/10.1029/2020JG005826>, 2021.

1120 Peterson, E. L.: Benthic shear stress and sediment condition, *Aquac. Eng.*, 21, 2, 85–111,
1121 [https://doi.org/10.1016/S0144-8609\(99\)00025-4](https://doi.org/10.1016/S0144-8609(99)00025-4), 1999.

1122 Pihlainen, S., Zandersen, M., Hyytiäinen, K., Andersen, H. E., Bartosova, A., Gustafsson, B.,
1123 Jabloun, M., McCrackin, M., Meier, H. E. M., Olesen, J. E., Saraiva, S., Swaney, D., and
1124 Thodsen, H.: Impacts of changing society and climate on nutrient loading to the Baltic Sea,
1125 *Sci. Tot. Env.*, 731, 138935, <https://doi.org/10.1016/j.scitotenv.2020.138935>, 2020.

1126 Pozo Buil, M., Jacox, M. G., Fiechter, J., Alexander, M. A., Bograd, S. J., Curchitser, E. N.,
1127 Edwards, C. A., Rykaczewski, R. R., & Stock, C. A.: A Dynamically Downscaled Ensemble
1128 of Future Projections for the California Current System, *Front. Mar. Sci.*, 8, April, 1–18,
1129 <https://doi.org/10.3389/fmars.2021.612874>, 2021.

1130 Prudhomme, C., Reynard, N., & Crooks, S.: Downscaling of global climate models for flood
1131 frequency analysis: Where are we now?, *Hydrol. Process.*, 16, 1137–1150,
1132 <https://doi.org/10.1002/hyp.1054>, 2002.

1133 Reum, J. C. P., Blanchard, J. L., Holsman, K. K., Aydin, K., Hollowed, A. B., Hermann, A. J.,
1134 Cheng, W., Faig, A., Haynie, A. C., & Punt, A. E.: Ensemble Projections of Future Climate
1135 Change Impacts on the Eastern Bering Sea Food Web Using a Multispecies Size Spectrum
1136 Model, *Front. Mar. Sci.*, 7, March, 1–17, <https://doi.org/10.3389/fmars.2020.00124>, 2020.

1137 Ross, A. C., & Najjar, R. G.: Evaluation of methods for selecting climate models to simulate
1138 future hydrological change, *Clim. Change*, 157, 3–4, 407–428,
1139 <https://doi.org/10.1007/s10584-019-02512-8>, 2019.

1140 Ryabchenko, V. A., Karlin, L. N., Isaev, A. V., Vankevich, R. E., Eremina, T. R., Molchanov,
1141 M. S., & Savchuk, O. P.: Model estimates of the eutrophication of the Baltic Sea in the
1142 contemporary and future climate, *Oceanology*, 56, 1, 36–45,
1143 <https://doi.org/10.1134/S0001437016010161>, 2016.

1144 Saraiva, S., Markus Meier, H. E., Andersson, H., Höglund, A., Dieterich, C., Gröger, M.,
1145 Hordoir, R., & Eilola, K.: Baltic Sea ecosystem response to various nutrient load scenarios in
1146 present and future climates, *Clim. Dyn.*, 52, 5–6, 3369–3387, [https://doi.org/10.1007/s00382-](https://doi.org/10.1007/s00382-018-4330-0)
1147 018-4330-0, 2019a.

1148 Saraiva, S., Markus Meier, H. E., Andersson, H., Höglund, A., Dieterich, C., Gröger, M.,
1149 Hordoir, R., & Eilola, K.: Uncertainties in projections of the Baltic Sea ecosystem driven by
1150 an ensemble of global climate models, *Front. Earth Sci.*, 6, January, 1–18,
1151 <https://doi.org/10.3389/feart.2018.00244>, 2019b.

1152 Schaefer, S. C., & Alber, M.: Temperature controls a latitudinal gradient in the proportion of
1153 watershed nitrogen exported to coastal ecosystems, *Biogeochemistry*, 85, 3, 333–346,
1154 <https://doi.org/10.1007/s10533-007-9144-9>, 2007.

1155 Shchepetkin, A. F. and McWilliams, J. C.: The Regional Oceanic Modeling System (ROMS): A
1156 Split-Explicit, Free-Surface, Topography-Following-Coordinate Oceanic Model, *Ocean*
1157 *Modelling*, 9, 347–404, <https://doi.org/10.1016/j.ocemod.2004.08.002>, 2005.

1158 Shenk, G., M. Bennett, D. Boesch, L. Currey, M. Friedrichs, M. Herrmann, R. Hood, T. Johnson,
1159 L. Linker, A. Miller, and D. Montali. 2021a. Chesapeake Bay Program Climate Change
1160 Modeling 2.0 Workshop. STAC Publication Number 21-003, Edgewater, MD. 35 pp.

1161 Shenk, G. W., Bhatt, G., Tian, R., Cerco, C.F., Bertani, I., Linker, L.C., 2021b. Modeling
1162 Climate Change Effects on Chesapeake Water Quality Standards and Development of 2025
1163 Planning Targets to Address Climate Change. CBPO Publication Number 328-21, Annapolis,
1164 MD. 145 pp.

1165 Siedlecki, S. A., Pilcher, D., Howard, E. M., Deutsch, C., MacCready, P., Norton, E. L., Frenzel,
1166 H., Newton, J., Feely, R. A., Alin, S. R., & Klinger, T.: Coastal processes modify projections
1167 of some climate-driven stressors in the California Current System, *Biogeosciences*, 18, 9,
1168 2871–2890, <https://doi.org/10.5194/bg-18-2871-2021>, 2021.

1169 Sinha, E., Michalak, A. M., & Balaji, V.: Eutrophication will increase during the 21st century as
1170 a result of precipitation changes, *Science*, 357, 6349, 1–5,
1171 <https://doi.org/10.1126/science.aan2409>, 2017.

1172 Springer, G. S., Dowdy, H. S., & Eaton, L. S.: Sediment budgets for two mountainous basins
1173 affected by a catastrophic storm: Blue ridge mountains, Virginia, *Geomorphology*, 37, 1–2,
1174 135–148, [https://doi.org/10.1016/S0169-555X\(00\)00066-0](https://doi.org/10.1016/S0169-555X(00)00066-0), 2001.

1175 St-Laurent, P., Friedrichs, M. A. M., Najjar, R. G., Shadwick, E. H., Tian, H., & Yao, Y.:
1176 Relative impacts of global changes and regional watershed changes on the inorganic carbon
1177 balance of the Chesapeake Bay, *Biogeosciences*, 17, 14, 3779–3796,
1178 <https://doi.org/10.5194/bg-17-3779-2020>, 2020.

1179 Tango, P. J., & Batiuk, R. A.: Chesapeake Bay recovery and factors affecting trends: Long-term
1180 monitoring, indicators, and insights, *Reg. Stu. in Mar. Sci.*, 4, 12-20,
1181 <https://doi.org/10.1016/j.rsma.2015.11.010>, 2016.

1182 Tebaldi, C., Arblaster, J. M., & Knutti, R.: Mapping model agreement on future climate
1183 projections, *Geophys. Res. Lett.*, 38, 23, 1–5, <https://doi.org/10.1029/2011GL049863>, 2011.

1184 Testa, J. M., Basenback, N., Shen, C., Cole, K., Moore, A., Hodgkins, C., & Brady, D. C.:
1185 Modeling Impacts of Nutrient Loading, Warming, and Boundary Exchanges on Hypoxia and
1186 Metabolism in a Shallow Estuarine Ecosystem, *J. Am. Water Resour. Assoc.*, 1–22,
1187 <https://doi.org/10.1111/1752-1688.12912>, 2021.

1188 Testa, J. M., Murphy, R. R., Brady, D. C., & Kemp, W. M.: Nutrient-and climate-induced shifts
1189 in the phenology of linked biogeochemical cycles in a temperate estuary, *Front. Mar. Sci.*, 5,
1190 114, <https://doi.org/10.3389/fmars.2018.00114>, 2018.

1191 Tian, R., Cerco, C. F., Bhatt, G., Linker, L. C., & Shenk, G. W.: Mechanisms Controlling
1192 Climate Warming Impact on the Occurrence of Hypoxia in Chesapeake Bay, *J. Am. Water
1193 Resour. Assoc.*, 1–21, <https://doi.org/10.1111/1752-1688.12907>, 2021.

1194 USEPA (U.S. Environmental Protection Agency): Chesapeake Bay Total Maximum Daily Load
1195 for Nitrogen, Phosphorus and Sediment. Annapolis, MD: U.S. Environmental Protection
1196 Agency Chesapeake Bay Program Office. [http://www.epa.gov/
1197 reg3wapd/tmdl/ChesapeakeBay/tmdlexec.html](http://www.epa.gov/reg3wapd/tmdl/ChesapeakeBay/tmdlexec.html), 2010.

1198 Vetter, T., Reinhardt, J., Flörke, M., van Griensven, A., Hattermann, F., Huang, S., Koch, H.,
1199 Pechlivanidis, I. G., Plötner, S., Seidou, O., Su, B., Vervoort, R. W., & Krysanova, V.:
1200 Evaluation of sources of uncertainty in projected hydrological changes under climate change
1201 in 12 large-scale river basins, *Clim. Change*, 141, 3, 419–433,
1202 <https://doi.org/10.1007/s10584-016-1794-y>, 2017.

1203 Wade, A. J., Skeffington, R. A., Couture, R.-M., Erlandsson Lampa, M., Groot, S., Halliday, S.
1204 J., Harezlak, V., Hejzlar, J., Jackson-Blake, L. A., Lepistö, A., Papastergiadou, E., Riera, J.
1205 L., Rankinen, K., Shahgedanova, M., Trolle, D., Whitehead, P. G., Psaltopoulos, D., &
1206 Skuras, D.: Land Use Change to Reduce Freshwater Nitrogen and Phosphorus will Be
1207 Effective Even with Projected Climate Change, *Water*, 14, 5, 829,
1208 <https://doi.org/10.3390/w14050829>, 2022.

1209 Wagena, M. B., Collick, A. S., Ross, A. C., Najjar, R. G., Rau, B., Sommerlot, A. R., Fuka, D.
1210 R., Kleinman, P. J. A., & Easton, Z. M.: Impact of climate change and climate anomalies on
1211 hydrologic and biogeochemical processes in an agricultural catchment of the Chesapeake
1212 Bay watershed, USA, *Sci. Total Environ.*, 637–638, 1443–1454,
1213 <https://doi.org/10.1016/j.scitotenv.2018.05.116>, 2018.

1214 Wählström, I., Höglund, A., Almroth-Rosell, E., MacKenzie, B. R., Gröger, M., Eilola, K.,
1215 Plikshs, M., & Andersson, H. C.: Combined climate change and nutrient load impacts on
1216 future habitats and eutrophication indicators in a eutrophic coastal sea, *Limnol. Oceanogr.*,
1217 1–18, <https://doi.org/10.1002/lno.11446>, 2020.

1218 Wakelin, S. L., Artioli, Y., Holt, J. T., Butenschön, M., & Blackford, J.: Controls on near-bed
1219 oxygen concentration on the Northwest European Continental Shelf under a potential future
1220 climate scenario, *Prog. Oceanogr.*, 93, 2020.

1221 Wang, H. M., Chen, J., Xu, C. Y., Zhang, J., & Chen, H.: A Framework to Quantify the
1222 Uncertainty Contribution of GCMs Over Multiple Sources in Hydrological Impacts of
1223 Climate Change, *Earth's Futur.*, 8, 8, <https://doi.org/10.1029/2020EF001602>, 2020.

1224 Wang, P., Linker, L., Wang, H., Bhatt, G., Yactayo, G., Hinson, K.E., & Tian, R.: Assessing
1225 water quality of the Chesapeake Bay by the impact of sea level rise and warming, *IOP Conf.*
1226 *Ser. Earth Environ. Sci.*, 82, 1, <https://doi.org/10.1088/1755-1315/82/1/012001>, 2017.

1227 Whitney, M. M., & Vlahos, P.: Reducing Hypoxia in an Urban Estuary despite Climate
1228 Warming, *Environ. Sci. Technol.*, 55, 2, 941–951, <https://doi.org/10.1021/acs.est.0c03964>,
1229 2021.

1230 Whitney, M.M.: Observed and projected global warming pressure on coastal hypoxia,
1231 *Biogeosciences*, 19, 4479–4497, <https://doi.org/10.5194/bg-19-4479-2022>, 2022.

1232 Wolkovich, E. M., Cook, B. I., Allen, J. M., Crimmins, T. M., Betancourt, J. L., Travers, S. E.,
1233 Pau, S., Regetz, J., Davies, T. J., Kraft, N. J. B., Ault, T. R., Bolmgren, K., Mazer, S. J.,
1234 McCabe, G. J., McGill, B. J., Parmesan, C., Salamin, N., Schwartz, M. D., & Cleland, E. E.:
1235 Warming experiments underpredict plant phenological responses to climate change, *Nature*,
1236 485, 7399, 494–497, <https://doi.org/10.1038/nature11014>, 2012.

1237 Wood, A. W., Leung, L. R., Sridhar, V., & Lettenmaier, D. P.: Hydrologic implications of
1238 dynamical and statistical approaches to downscaling climate model outputs, *Clim. Change*,
1239 62, 1–3, 189–216, <https://doi.org/10.1023/B:CLIM.0000013685.99609.9e>, 2004.

1240 Xu, J., Long, W., Wiggert, J. D., Lanerolle, L. W. J., Brown, C. W., Murtugudde, R., and Hood,
1241 R. R.: Climate Forcing and Salinity Variability in Chesapeake Bay, USA, *Estuaries and*
1242 *Coasts*, 35, 237–261, <https://doi.org/10.1007/s12237-011-9423-5>, 2011.

1243 Yang, Q., Tian, H., Friedrichs, M. A. M., Liu, M., Li, X., & Yang, J.: Hydrological responses to
1244 climate and land-use changes along the north american east coast: A 110-Year historical
1245 reconstruction, *J. Am. Water Resour. Assoc.*, 51, 1, 47–67,
1246 <https://doi.org/10.1111/jawr.12232>, 2015.

1247 Yang, X., Wang, X., Cai, Z., & Cao, W.: Detecting spatiotemporal variations of maximum
1248 rainfall intensities at various time intervals across Virginia in the past half century, *Atmos.*
1249 *Res.*, 255, <https://doi.org/10.1016/j.atmosres.2021.105534>, 2021.

1250 Yao, Y., Tian, H., Pan, S., Najjar, R. G., Friedrichs, M. A. M., Bian, Z., Li, H. Y., & Hofmann,
1251 E. E.: Riverine Carbon Cycling Over the Past Century in the Mid-Atlantic Region of the
1252 United States, *J. Geophys. Res. Biogeosciences*, 126, 5, 1–21,
1253 <https://doi.org/10.1029/2020JG005968>, 2021.

1254 Yau, Y. Y., Baker, D. M., & Thibodeau, B.: Quantifying the Impact of Anthropogenic
1255 Atmospheric Nitrogen Deposition on the Generation of Hypoxia under Future Emission
1256 Scenarios in Chinese Coastal Waters, *Environ. Sci. Technol.*, 54, 7, 3920–3928,
1257 <https://doi.org/10.1021/acs.est.0c00706>, 2020.

1258 Yip, S., Ferro, C. A. T., Stephenson, D. B., & Hawkins, E.: A Simple, coherent framework for
1259 partitioning uncertainty in climate predictions, *J. Clim.*, 24, 17, 4634–4643,
1260 <https://doi.org/10.1175/2011JCLI4085.1>, 2011.

1261 Zahran, A. R., Zhang, Q., Tango, P., & Smith, E. P.: A water quality barometer for Chesapeake
1262 Bay: Assessing spatial and temporal patterns using long-term monitoring data, *Ecol. Indic.*,
1263 140, April, 109022, <https://doi.org/10.1016/j.ecolind.2022.109022>, 2022.

1264 Zhang, Q., Murphy, R. R., Tian, R., Forsyth, M. K., Trentacoste, E. M., Keisman, J., & Tango, P.
1265 J.: Chesapeake Bay's water quality condition has been recovering: Insights from a
1266 multimetric indicator assessment of thirty years of tidal monitoring data, *Sci. Total Environ.*,
1267 637–638, 1617–1625, <https://doi.org/10.1016/j.scitotenv.2018.05.025>, 2018.
1268 Zhang, W., Dunne, J. P., Wu, H., & Zhou, F.: Regional projection of climate warming effects on
1269 coastal seas in east China, *Environ. Res. Lett.*, 17, 7, 074006, [https://doi.org/10.1088/1748-](https://doi.org/10.1088/1748-9326/ac7344)
1270 9326/ac7344, 2022.
1271 Zhang, W., Moriarty, J. M., Wu, H., & Feng, Y.: Response of bottom hypoxia off the Changjiang
1272 River Estuary to multiple factors: A numerical study, *Ocean Model.*, 159, May 2020,
1273 <https://doi.org/10.1016/j.ocemod.2021.101751>, 2021.
1274

1275 **Tables and Figures**

1276

1277 **Table 1.** Experiments conducted to quantify future changes in Annual Hypoxic Volume (AHV).

1278

Experiment Name	Number of ESMs	Number of downscaling techniques	Number of watershed models	Number of simulations
Multi-Factor	5 ^a	2 (MACA and BCSD)	2 (DLEM and Phase 6)	20 ^b
Management	5 ^a	1 (MACA)	1 (Phase 6)	5 ^c
All-ESMs	20	1 (MACA)	1 (DLEM)	20

1279 ^aCorresponding to the KKZ-selected subset of five ESMs: Center, Cool/Dry, Hot/Wet, Cool/Wet, and Hot/Dry for both MACA
 1280 and BCSD downscaled model outputs.

1281 ^bAdditional scenarios were simulated for the Multi-Factor experiment as needed (for the Center and Hot/Wet ESMs) to
 1282 accurately partition uncertainty in model outcomes.

1283 ^cAn additional scenario simulated the effects of future management conditions without climate change impacts.

1284 **Table 2:** Nash-Sutcliffe efficiencies of the DLEM and Phase 6 Watershed Models at the most
 1285 downstream stations of three major rivers, for monthly estimates of discharge and nutrient
 1286 loading over the period 1991-2000. Nash-Sutcliffe efficiencies equal to one are indicative of
 1287 perfect model skill and negative values indicate that error variance exceeds the observed
 1288 variance.

Major River	Freshwater Discharge		Nitrate Loading		Organic Nitrogen Loading	
	DLEM	Phase 6	DLEM	Phase 6	DLEM	Phase 6
Susquehanna	0.74	0.88	0.60	0.78	0.37	0.12
Potomac	0.59	0.90	0.32	0.87	0.34	-0.69
James	0.59	0.92	-1.05	0.42	0.51	0.72

1289

1290 **Table 3:** Model skill metrics over the reference period (1991-2000)

Variable	Depth	Watershed model	ChesROMS-ECB estimate	Observed estimate ^a	Bias	RMSD
O ₂ [mg L ⁻¹]	Surface	DLEM	7.9 ± 2.3	9.3 ± 2.0	-1.4	2.2
		Phase 6	8.0 ± 2.3		-1.4	2.2
	Bottom	DLEM	6.1 ± 3.5	5.7 ± 3.5	0.4	1.7
		Phase 6	6.2 ± 3.4		0.5	1.6
NO ₃ [mmol N m ³]	Surface	DLEM	0.32 ± 0.36	0.23 ± 0.33	0.09	0.23
		Phase 6	0.30 ± 0.37		0.06	0.22
	Bottom	DLEM	0.27 ± 0.33	0.14 ± 0.24	0.13	0.25
		Phase 6	0.25 ± 0.33		0.11	0.23
DON [mmol N m ³]	Surface	DLEM	0.27 ± 0.05	0.28 ± 0.08	-0.00	0.08
		Phase 6	0.32 ± 0.08		0.05	0.12
	Bottom	DLEM	0.27 ± 0.05	0.26 ± 0.08	0.00	0.08
		Phase 6	0.31 ± 0.08		0.04	0.11
Primary Production [mg C m ⁻² d ⁻¹]	Water	DLEM	1146 ± 154 ^b	957 ± 287	189	N/A
	Column	Phase 6	1133 ± 129		176	
AHV [km ³ d]	Water	DLEM	987 ± 254	785 ± 201	202	250
	Column	Phase 6	906 ± 199		121	212

1291 ^aObserved estimates and standard deviations for O₂, NO₃, and DON are from Water Quality Monitoring Program data at 20 main
1292 stem stations. Observed estimate and standard error for primary production are derived from Harding et al. (2002), averaged over
1293 Feb-Nov for the years 1982-1998. Observed estimate and standard deviation for AHV is derived by applying a weighted-distance
1294 interpolation model to observed O₂ at a limited number of stations (Bever et al., 2013).

1295 ^bModeled primary production is computed only over Feb-Nov for comparison with the observed estimate.

1296
1297

Table 4: Annual average and standard deviations of reference (1991-2000) and climate scenario (2046-2055) watershed loadings and estuarine hypoxia.

Watershed Freshwater Discharge [km ³ y ⁻¹]					
Watershed Model	DLEM		Phase 6		Phase 6 with Management
1990s	84 ± 26		72 ± 21		74 ± 21
2050s Downscaling	MACA	BCSD	MACA	BCSD	MACA
Center	87 ± 28	74 ± 24	78 ± 21	80 ± 22	79 ± 21
Cool/Dry	76 ± 24	75 ± 24	67 ± 19	77 ± 22	68 ± 19
Hot/Wet	84 ± 29	86 ± 29	79 ± 22	77 ± 21	80 ± 22
Hot/Dry	77 ± 25	74 ± 23	70 ± 20	68 ± 20	72 ± 20
Cool/Wet	93 ± 29	95 ± 30	83 ± 22	80 ± 22	84 ± 22
ESM Average	84 ± 27	81 ± 26	75 ± 21	76 ± 21	77 ± 21
Watershed Nitrogen Loading [10 ⁹ gN y ⁻¹]					
Watershed Model	DLEM		Phase 6		Phase 6 with Management
1990s	151 ± 49		147 ± 46		87 ± 28
2050s Downscaling	MACA	BCSD	MACA	BCSD	MACA
Center	159 ± 46	138 ± 41	177 ± 63	192 ± 75	103 ± 36
Cool/Dry	137 ± 39	132 ± 38	133 ± 36	166 ± 53	78 ± 23
Hot/Wet	157 ± 48	153 ± 45	183 ± 66	184 ± 68	105 ± 37
Hot/Dry	149 ± 45	138 ± 41	146 ± 42	140 ± 40	86 ± 26
Cool/Wet	159 ± 43	181 ± 62	301 ± 186	352 ± 244	156 ± 85
ESM Average	152 ± 43	148 ± 48	188 ± 110	207 ± 139	105 ± 53
Annual Hypoxic Volume [km ³ d]					
Watershed Model	DLEM		Phase 6		Phase 6 with Management
1990s	987 ± 254		904 ± 171		449 ± 144
2050s Downscaling	MACA	BCSD	MACA	BCSD	MACA
Center	1072 ± 233	985 ± 250	926 ± 152	938 ± 152	470 ± 131
Cool/Dry	994 ± 252	975 ± 257	885 ± 177	961 ± 170	429 ± 148
Hot/Wet	1094 ± 247	1059 ± 249	931 ± 156	928 ± 171	480 ± 131
Hot/Dry	1075 ± 263	996 ± 259	893 ± 164	871 ± 165	442 ± 141
Cool/Wet	1011 ± 204	1081 ± 238	969 ± 170	997 ± 203	507 ± 138
ESM Average	1049 ± 234	1019 ± 244	921 ± 160	939 ± 171	466 ± 135

1298

1299 **Table 5:** Average \pm standard error in Δ AHV (%) holding scenario effects (ESM, Downscaling
 1300 Method, Watershed Model) constant.

Scenario Factor	Effect	Δ AHV ₁₃₀₁ %
ESM	Center	4.4 \pm 5.4
	Cool/Dry	0.9 \pm 4.3
	Hot/Wet	6.7 \pm 6.2
	Hot/Dry	1.4 \pm 3.6
	Cool/Wet	8.3 \pm 6.5
Downscaling	MACA	4.8 \pm 6.0
	BCSD	3.9 \pm 5.9
Watershed Model	DLEM	5.6 \pm 7.5
	Phase 6	3.1 \pm 3.8

Table 6: A summary comparison of simulated mid-21st century climate change impacts on Chesapeake Bay hypoxia relative to observed conditions.

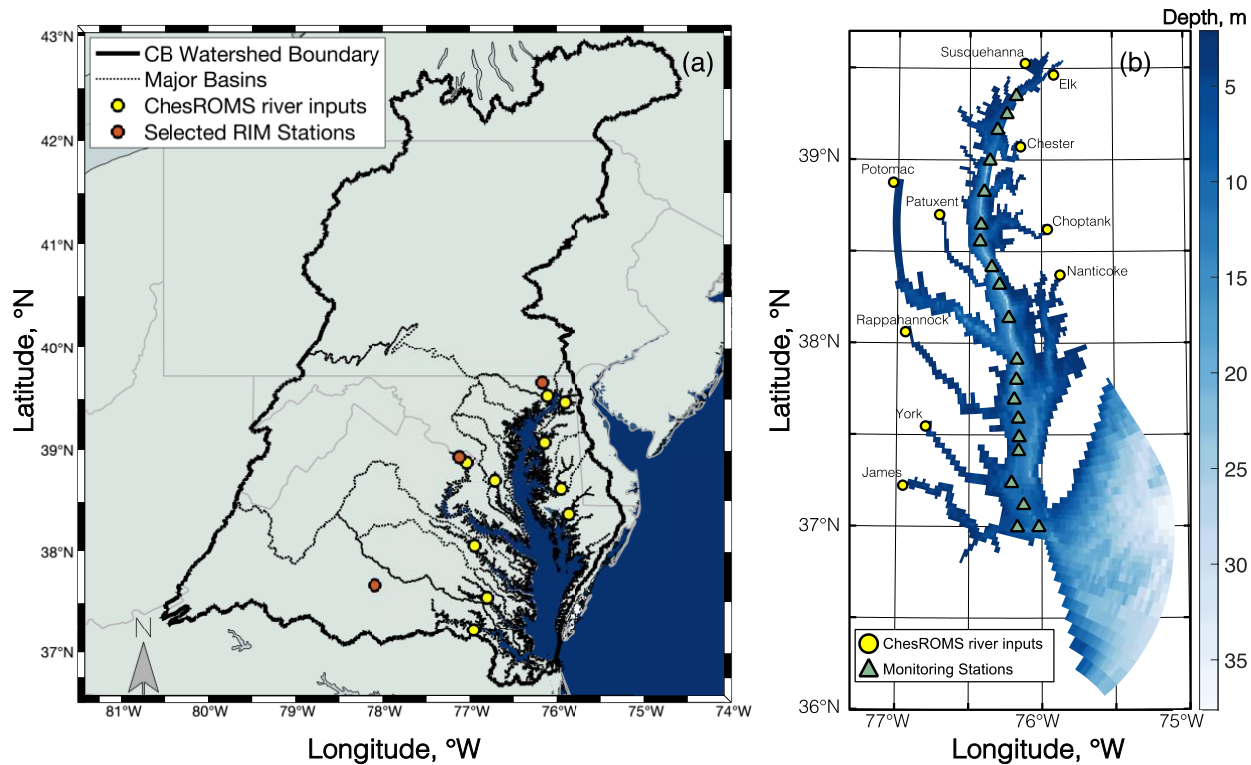
Published Research	Climate Change Factors	Future Oxygen Change
Watershed Changes		
Wang et al., 2017	Increased watershed nitrogen loadings by +5 to +10%	No AHV estimate provided Increase in AAV*: +9.7 to +18.7%
Irby et al., 2018	Changed watershed discharge by -2% to +17% (varying by month); assumed nutrient reductions	Increase in AHV: +5%
Hinson et al., 2023** (this paper)	Changed watershed loadings according to two watershed models, two downscaling techniques, and five ESMs	Increase in AHV: +4.4 ± 7.4% Increase in AAV: +10.0 ± 16.5%
Temperature Changes		
Irby et al., 2018	Increased estuarine temperatures by 1.75 °C; assumed nutrient reductions	Increase in AHV: +13%
Tian et al., 2021	Increased atmosphere and ocean temperature increased by ~1 °C	†Increase in AHV: +9%
Sea Level Rise		
Irby et al., 2018	Increased sea level by 0.5 m; assumed nutrient reductions	Decrease in AHV: -13%
St-Laurent et al. 2019	Increased sea level by 0.5 m for 4 different models	Increase in summertime bottom O ₂ in all 4 models
Cai et al., 2022	Increased sea level by 0.5 m	Increase in AHV by +8%
Cerco and Tian, 2022	Increased sea level by 0.22 to 1 m and simulated wetland losses	Increase in DO criteria exceedances
Multiple Environmental Changes		
Irby et al. 2018	Combined atmosphere, watershed and sea level change, assuming nutrient reductions	Increase in AHV: +9%
Ni et al., 2019**	Combined atmosphere, watershed, and ocean Change: Multiple downscaled scenarios that increased air temperatures, monthly discharge, ocean temperatures and sea surface height	Increase in AHV: +9 to 31% Increase in AAV: +2 to 29%
Basenback et al., 2022	Modified timing of nutrient delivery and warming within the estuary	Change in AHV: -10% to +18%

AAV = Annual Anoxic Volume; AHV = Annual Hypoxic Volume

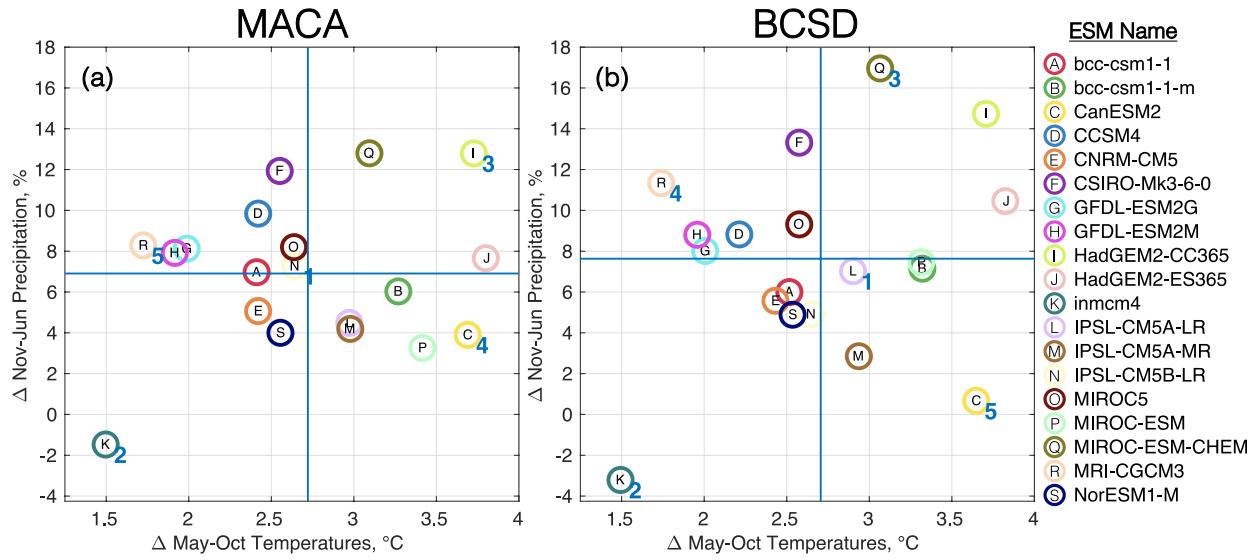
*AAV defined as O₂ < 1 mg L⁻¹ in Wang et al. (2017), and O₂ < 0.2 mg L⁻¹ for all others.

**Applied downscaled ESMs in projecting changes to Chesapeake Bay hypoxia.

†No 2050 estimate provided; results based on 2025 projected changes.

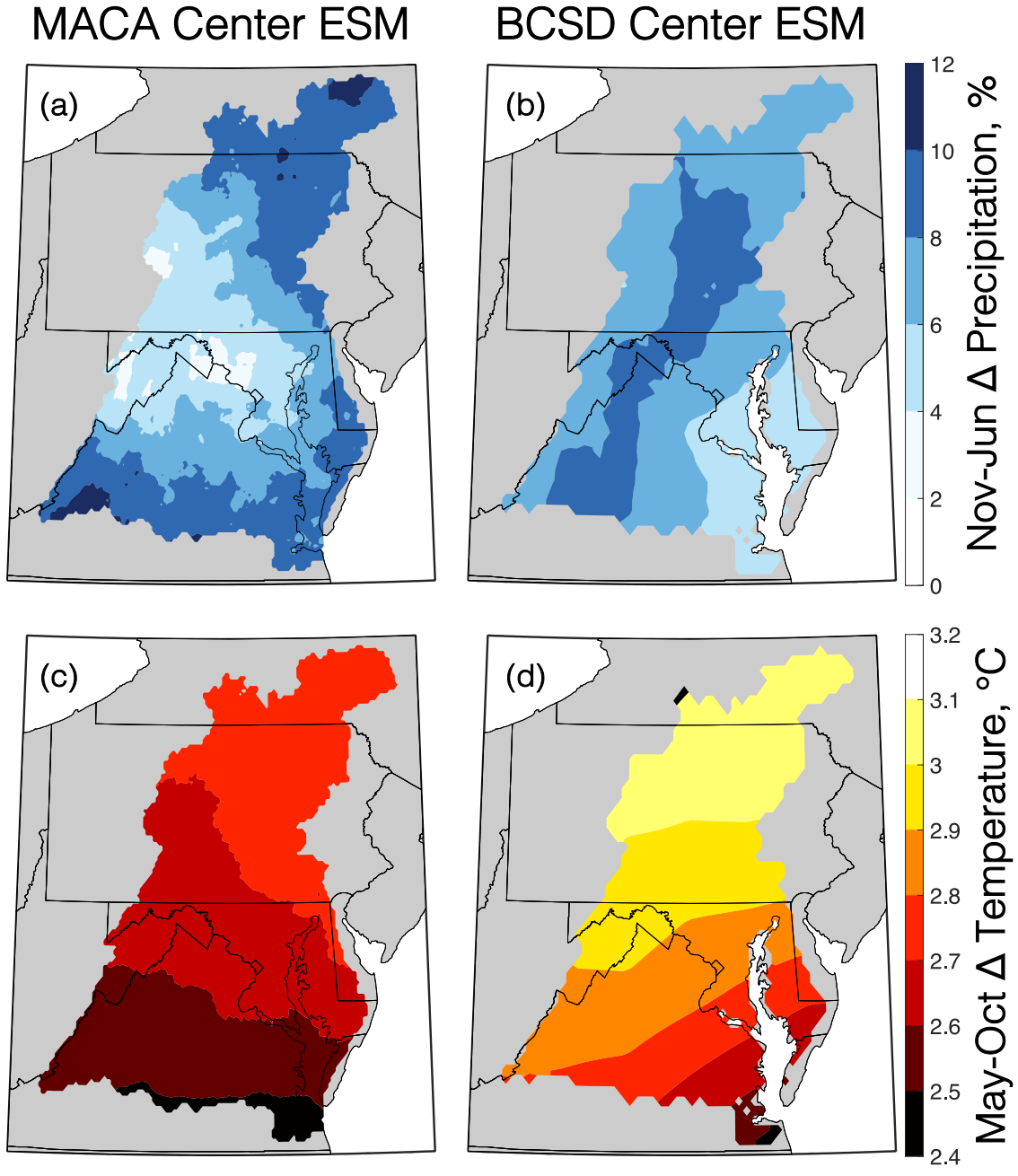


1302
 1303 **Figure 1:** (a) Map showing the extent of the Chesapeake Bay watershed boundary, major basins,
 1304 River Input Monitoring stations for the Susquehanna, Potomac, and James Rivers (red circles),
 1305 and ChesROMS-ECB river input locations (yellow circles). (b) Bathymetry of the ChesROMS-
 1306 ECB model domain, river input locations (yellow circles), and 20 Chesapeake Bay Program
 1307 main stem monitoring stations (green triangles).



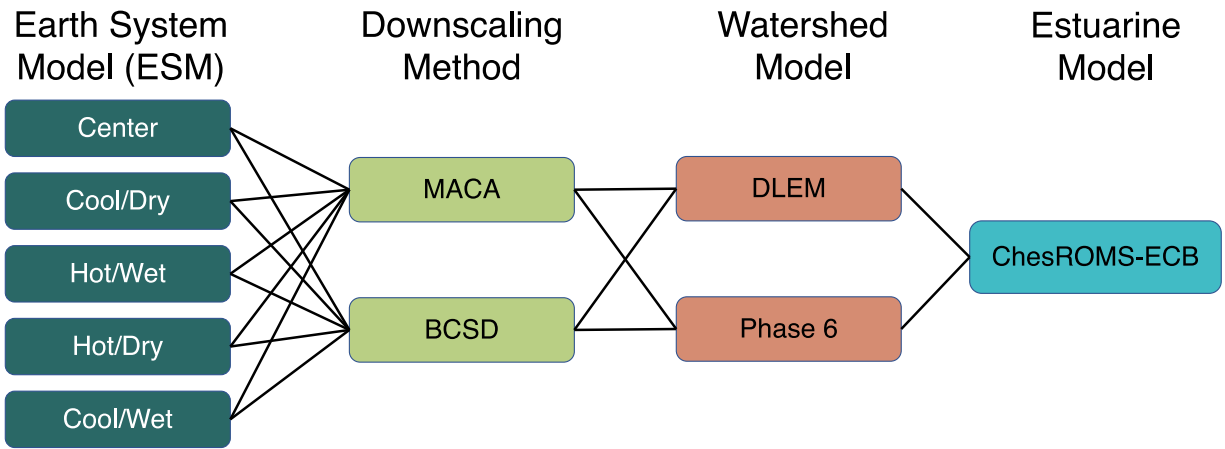
1308
 1309
 1310
 1311
 1312
 1313

Figure 2: Relative changes in May-October temperatures and November-June precipitation over the Chesapeake Bay watershed for an ensemble of ESMs (circled letters) downscaled using (a) MACA and (b) BCSD methodologies. Horizontal and vertical blue lines correspond to the ensemble average changes in temperature and precipitation. Numbers adjacent to particular ESMs in both panels denote the order in which the first five were selected by the KKZ algorithm.



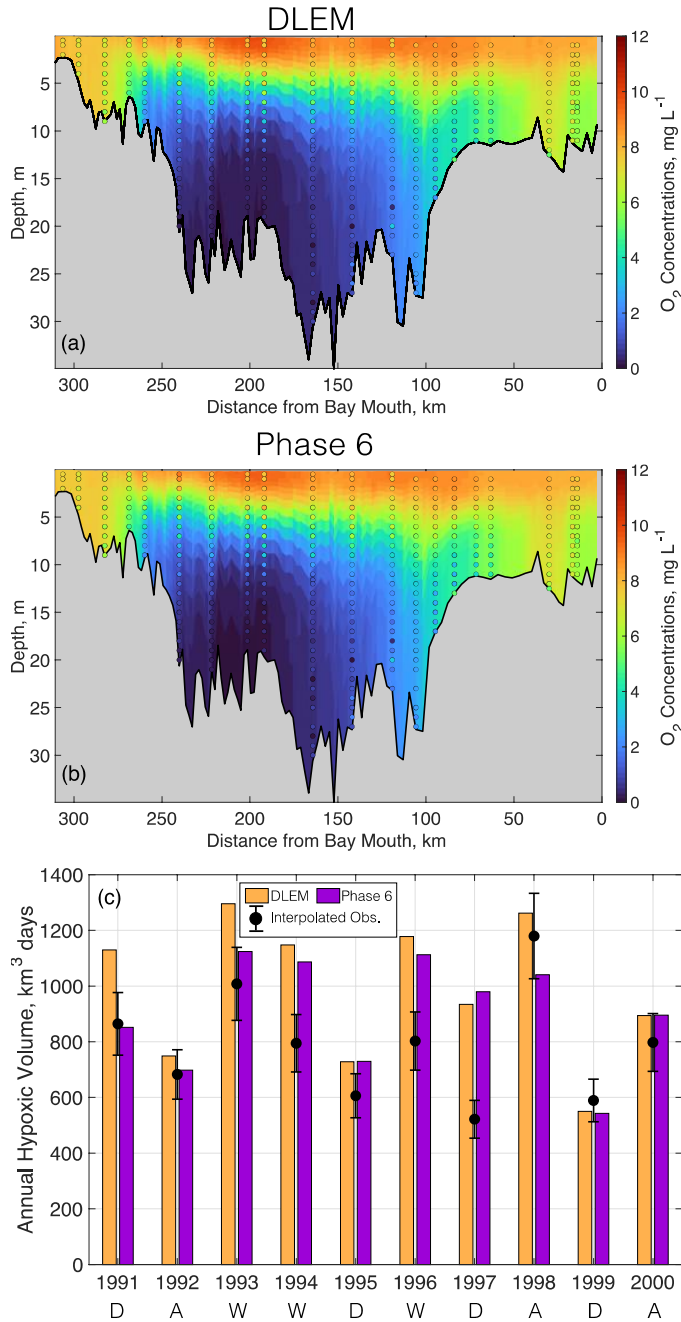
1314
 1315
 1316
 1317

Figure 3: Changes in November to June precipitation (a, b) and May to October temperatures (c, d) for the MACA (a, c) and BCSD (b, d) Center ESMs between mid-century (2046-2055) and the reference period (1991-2000).

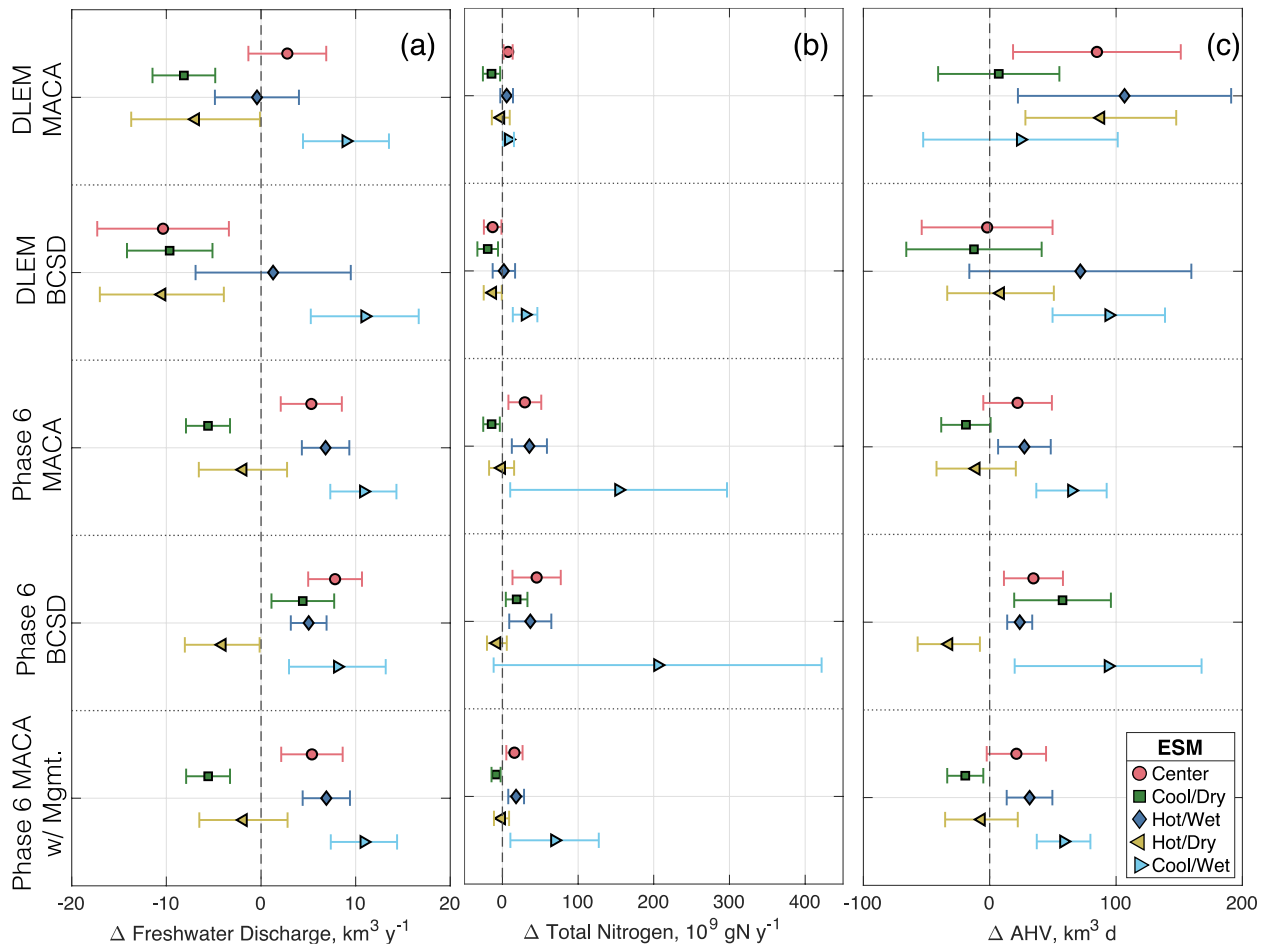


1318
 1319
 1320

Figure 4: Diagram of Multi-Factor experimental design, comprising a total of 20 model scenarios.

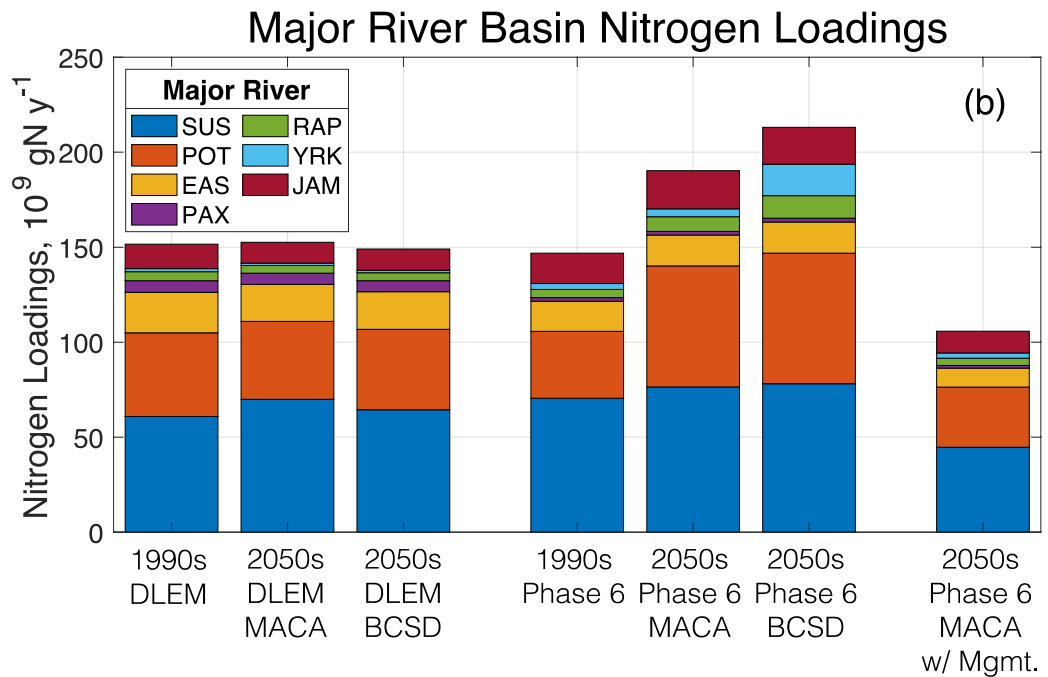
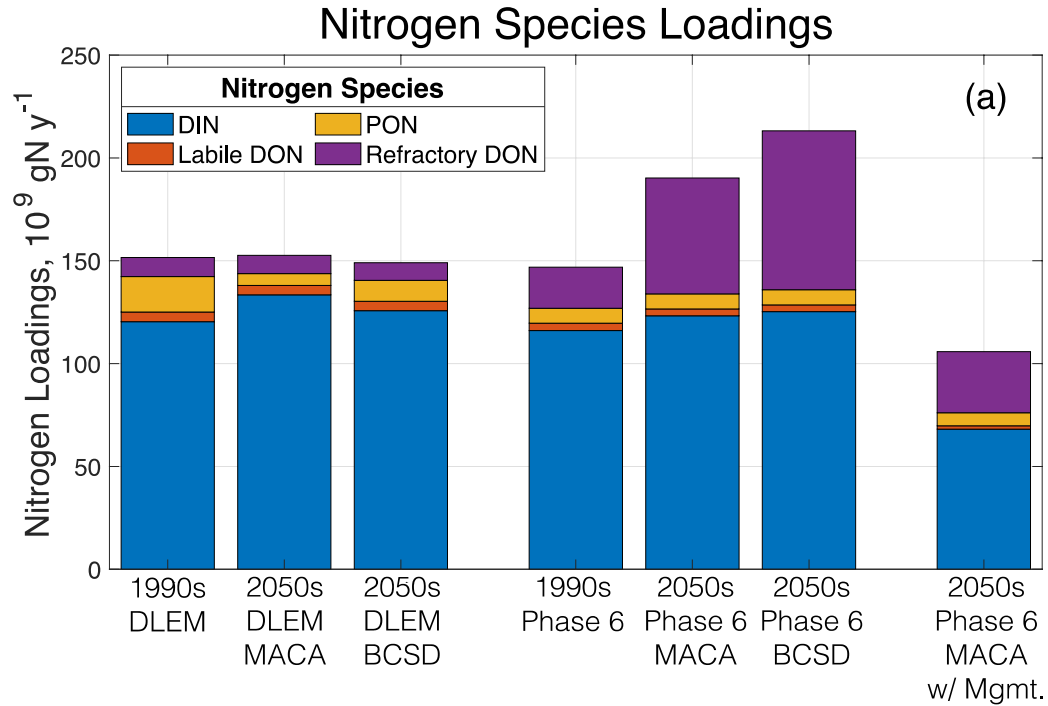


1321
 1322 **Figure 5:** ChesROMS-ECB skill for average summer (Jun-Aug) O₂ profiles at main stem
 1323 monitoring locations using watershed inputs from (a) DLEM and (b) Phase 6 over the reference
 1324 period 1991-2000. (c) Modeled AHV using DLEM and Phase 6 compared to interpolated
 1325 observations (error bars denote RMS percent error) over the reference period 1991-2000.
 1326 Average hydrologic conditions are noted below corresponding years and signify dry (D), average
 1327 (A), or wet (W) years.

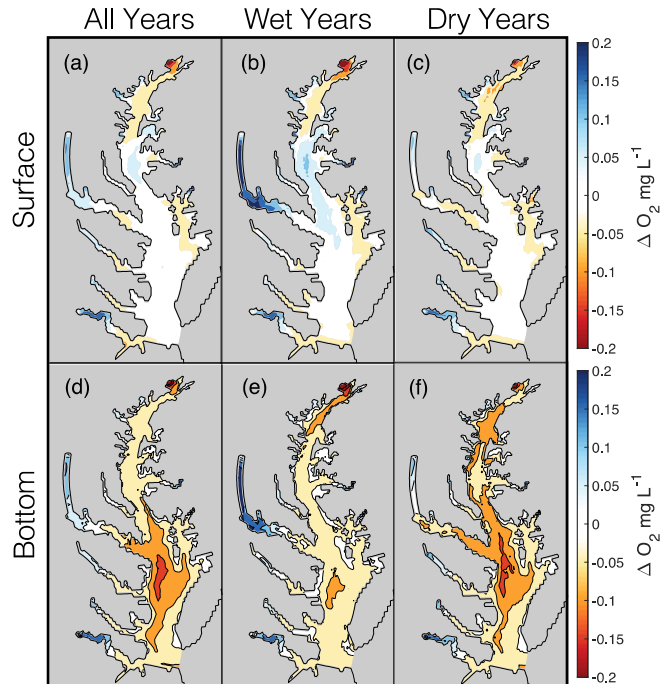


1329
1330

1331 **Figure 6:** Mean and standard deviations of changes to freshwater discharge (a), total nitrogen
 1332 loadings (b), and annual hypoxic volume (c) for Multi-Factor and Management experiments.
 1333 Future climate changes in these outputs are shown relative to 1990s baseline conditions (dashed
 1334 vertical line) without management actions (upper four rows) and with management
 1335 actions (bottom row).

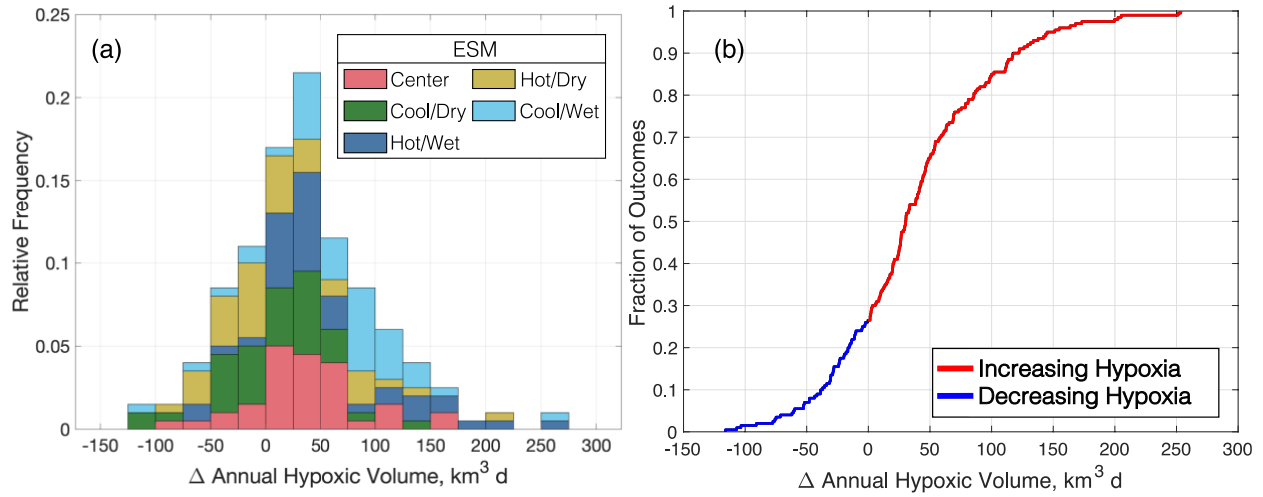


1336
 1337 **Figure 7:** Average total nitrogen loadings among ESM scenarios for reference scenarios and
 1338 various components of the Multi-Factor and Management experiments. Total nitrogen loadings
 1339 divided by (a) nitrogen species component: dissolved inorganic nitrogen (DIN), particulate
 1340 organic nitrogen (PON), dissolved organic nitrogen (DON), and refractory dissolved organic
 1341 nitrogen, and (b) by major river basin (SUS = Susquehanna, RAP = Rappahannock, POT =
 1342 Potomac, YRK = York, EAS denoting eastern shore rivers including the Elk, Chester, Choptank,
 1343 and Nanticoke, JAM = James, PAX = Patuxent).



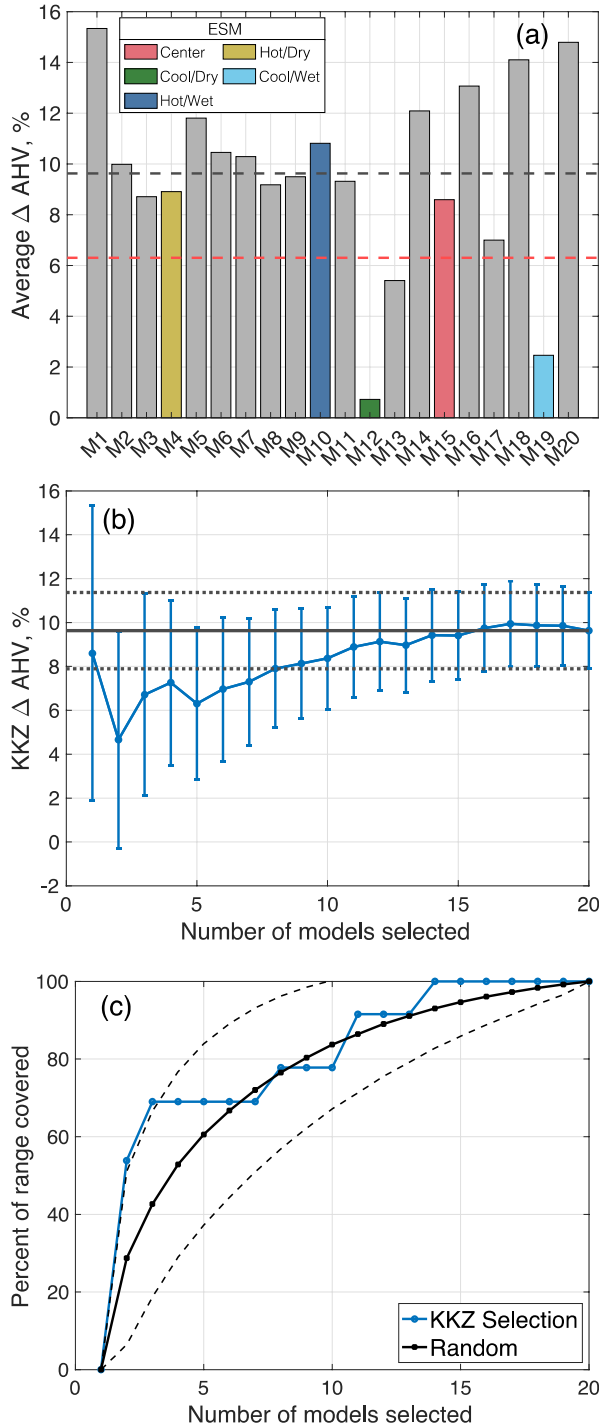
1344
 1345
 1346
 1347

Figure 8: Average O₂ changes in Multi-Factor experiment scenarios at the surface (a-c) and bottom (d-f). Columns correspond to average changes for all years (a, d) as well as hydrologically wet (b, e) and dry (c, f) years.

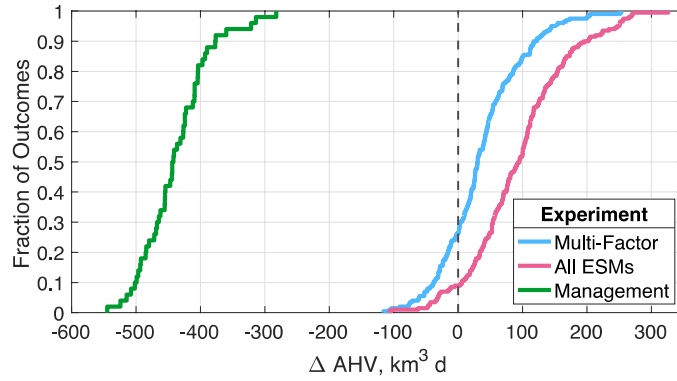


1348
1349
1350

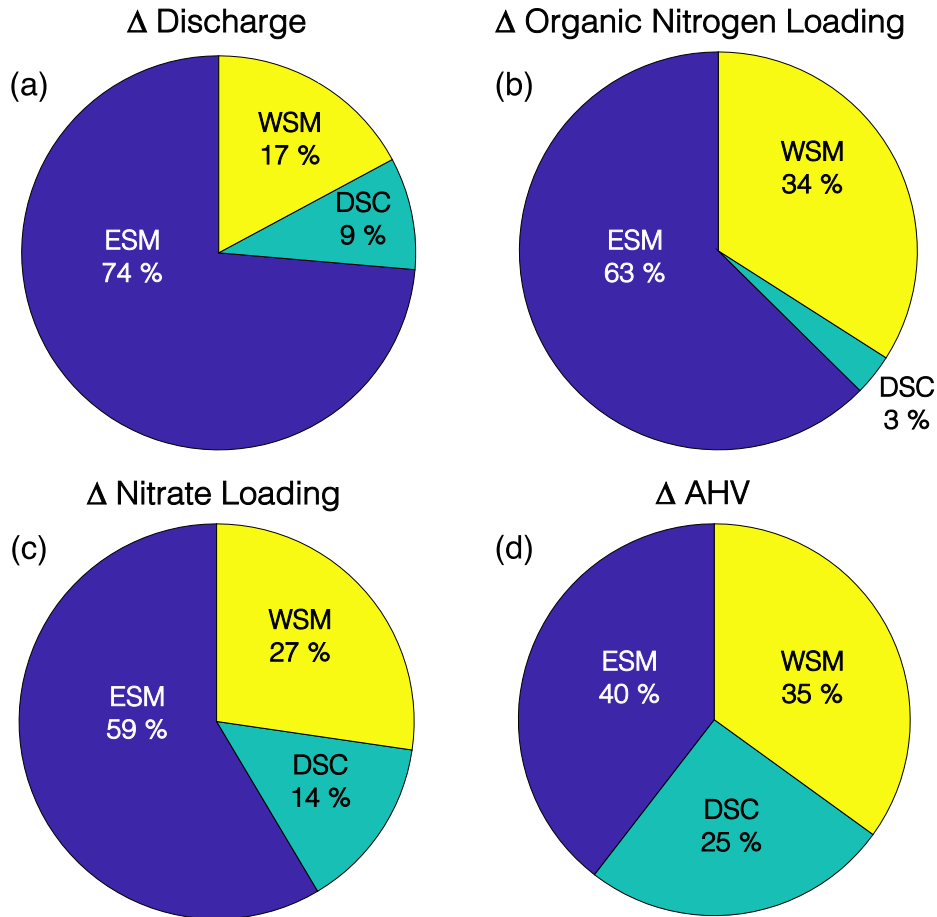
Figure 9: Summary of Multi-Factor experiment results for changes to Annual Hypoxic Volume, expressed as a histogram of relative frequencies (a) and an empirical cumulative distribution (b).



1351
 1352 **Figure 10:** (a) Change in Annual Hypoxic Volume (ΔAHV) for the All-ESMs experiment. Red
 1353 dashed line denotes the multi-model average of five KKZ-selected ESMs; black dashed line
 1354 denotes the full 20-model average. (b) ΔAHV and standard errors as estimated by increasing
 1355 number of KKZ-selected ESMs. Black lines correspond to 20-model average (solid) and
 1356 associated standard errors (dotted) from the All-ESMs experiment. (c) Percent of ΔAHV range
 1357 covered by sequentially increasing the number of KKZ-selected ESMs. Black lines correspond to
 1358 the range (solid) and associated standard error (dashed) of estimates chosen by randomly
 1359 selecting ESMs.



1360
 1361 **Figure 11:** Summary of all experiment results for change in Annual Hypoxic Volume (Δ AHV),
 1362 expressed as a cumulative distribution function. Black dashed vertical line corresponds to no
 1363 change in AHV.



1364
 1365
 1366
 1367

Figure 12: Percent contribution to uncertainty from Earth System Model (ESM), downscaling methodology (DSC), and watershed model (WSM), for estimates of (a) discharge, (b) organic nitrogen loading, (c) nitrate loading, and (d) change in annual hypoxic volume (Δ AHV).